buildings

MDPI

Article

Research on Integral Splicing Design and Construction Technology for Two Separate Spans of a Prestressed Concrete Continuous Rigid-Frame Bridge

Chunyao Zhong [1], Qiao Lu [1], Yangfan Li [1], Xuefei Shi [2,*], Jun Song [2] and Chaoyu Zhu [2]

[1] Guangdong Provincial Freeway Co., Ltd., Guangzhou 510620, China; yes19821004@163.com (C.Z.); gdfreewayluqiao@163.com (Q.L.); liyangfan2025@163.com (Y.L.)
[2] Department of Bridge Engineering, Tongji University, Shanghai 200092, China; songjun815@alumni.tongji.edu.cn (J.S.); zhuchaoyu@126.com (C.Z.)
* Correspondence: shixf@tongji.edu.cn

Abstract

For an existing bridge constructed with separate spans, the ends of adjacent flanges are disconnected. The problem of separated driving may occur at the bridgehead position after traffic conversion. The idea of integral splicing two separate spans of the existing long-span bridge is proposed. Direct crossing of a vehicle between the two separate spans of the existing long-span bridge can be realized. Firstly, the demand for integral splicing of the existing box girder bridge is analyzed using different methods. Then, an integral splicing composite structure (ISC-Structure) is designed and tested, and the corresponding design method is summarized. Finally, the construction technology for the ISC-Structure is optimized based on the actual field conditions. This research shows that the integral splicing demand of the old bridge can be obtained through on-site monitoring at the splicing position. Furthermore, the proposed random traffic flow simulation method can be applied to expand the data volume and verify the validity of the monitoring data. The proposed ISC-Structure meets the transverse splicing requirements of the Xinfengjiang Bridge. It can effectively connect the two separate spans, enabling them to work compositely and improving longitudinal mechanical properties. A layered and segmented construction scheme is proposed, and the relevant construction technology is optimized for the target integral splicing project. The proposed integral splicing design and construction technology can sever as a reference for similar long-span bridge extension projects.

Keywords: continuous rigid-frame bridge; two separate spans; integral splicing composite structure (ISC-Structure); design method; construction technology

check for updates

Academic Editor: Rajai Zuheir Al-Rousan

Received: 29 July 2025
Revised: 17 August 2025
Accepted: 2 September 2025
Published: 5 September 2025

Citation: Zhong, C.; Lu, Q.; Li, Y.; Shi, X.; Song, J.; Zhu, C. Research on Integral Splicing Design and Construction Technology for Two Separate Spans of a Prestressed Concrete Continuous Rigid-Frame Bridge. *Buildings* **2025**, *15*, 3208. https://doi.org/10.3390/buildings15173208

Copyright: © 2025 by the authors. Licensee MDPI, Basel, Switzerland. This article is an open access article distributed under the terms and conditions of the Creative Commons Attribution (CC BY) license (https://creativecommons.org/licenses/by/4.0/).

1. Introduction

In freeway reconstruction and extension projects, widening is typically performed on both sides or on one side only [1]. For long-span bridges crossing large rivers, the extension approach of building a new bridge on one side can be adopted to reduce the land occupation of the new bridge [2]. The new bridge carries traffic in one direction, and the old bridge carries traffic in the other direction, as shown in Figure 1.

However, for the existing bridge constructed with separate spans, the traffic lanes must remain separated on each span due to the disconnected ends of adjacent flanges. The problem of separated driving also occurs at the bridgehead position, which is prone to traffic accidents [3]. It is necessary to connect the two separate spans of the existing bridge

to ensure the safety of passing vehicles. Therefore, the concept of integral splicing for the existing bridges is proposed, as shown in Figure 1. It can be defined as implementing connections between the adjacent flange plates of the existing box girder bridge (constructed with separate spans), which can realize direct vehicle crossing.

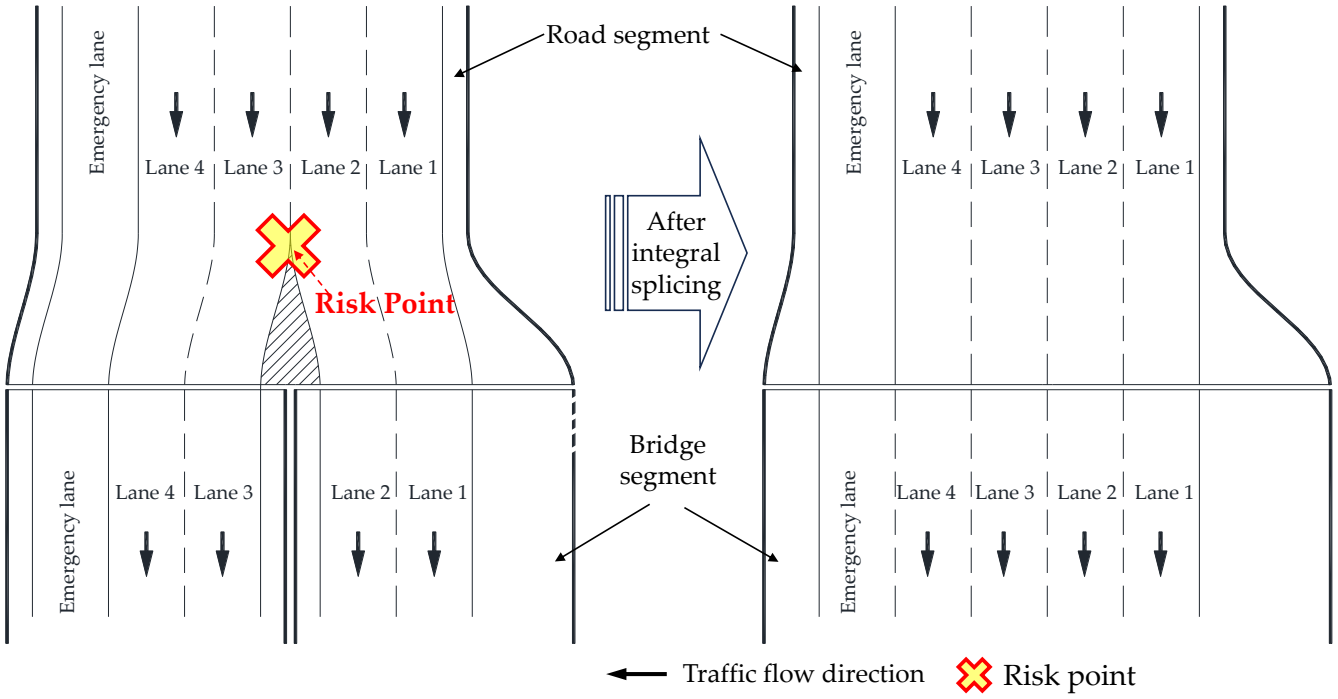


Figure 1. Problem of separated driving on a long-span bridge.

At the splicing position in an actual project, several layers are involved: the asphalt pavement layer, the integral layer, and the flange plate structure layer [4]. Existing research results have primarily focused on these layers, and virous bridge connection schemes have been proposed.

In existing research, studies have focused on disconnecting these layers, typically by adopting expansion joints. This approach results in an unconnected bridge deck and an unspliced structure. Krishna Mochtar et al. [5] conducted a literature review on the expansion capacity of different types of expansion joints and compared their unit price and installation time consumption. However, the expansion joints currently in use are primarily of the transverse type, which may not meet the requirements of the longitudinal expansion joints needed in this research. Li et al. [6] applied longitudinal expansion joints in a short-span wide bridge to reduce deck cracking caused by the temperature effects and shrinkage. Additionally, Li et al. [7] studied longitudinal and transverse cross-expansion joint structures in a short-span bridge extension project. This structure can also meet the requirements regarding the temperature effect and shrinkage, to some extent. Although longitudinal expansion joint structures can be selected for bridge expansion projects, they remain difficult to popularize. Because longitudinal expansion joints are parallel to the direction of the traffic and are mostly made of steel, problems, such as wheels becoming stuck or vehicle staggering and slipping, may occur when vehicles travel across them.

Conversely, connecting these layers should be adopted to ensure smoother traffic flows in actual projects. Depending on the width of the splicing joints, the connection schemes of the pavement layer (asphalt) and the integral layer or the flange plate structure layer (concrete) can be implemented. Wang et al. [8] applied high-elasticity asphalt concrete in the longitudinal joints of bridge widening. Swanson et al. [9] developed a material of silicone foam sealant for small-movement bridge expansion joints. Lu et al. [10] proposed a

type of polyurethane-modified asphalt to optimize bridge expansion joint interfaces. These new materials can be reasonably applied in widening bridges by virtue of their excellent deformation resistance. Therefore, the pavement layer connection schemes are limited to applications using small joint widths.

However, significant deformation differences may occur at the splicing position in long-span bridges. From a material perspective, whether these materials can accommodate large vertical deformation differences requires further investigation. Therefore, more studies have focused on structural connections. Tan et al. [11] and Chen et al. [12] studied different widening and splicing methods for medium-span and short-span bridges. These splicing methods offer valuable insights for splicing long-span bridges. Wu et al. [13,14] proposed different types of transverse splicing connection devices in the widening projects of a long-span continuous concrete box-girder bridge. These new solutions have been numerically analyzed, but not verified in actual projects. In addition, it is worth noting that studies have been conducted [15,16] to ensure structural splicing, specifically targeting uninterrupted traffic during splicing new and old bridges. Therefore, research on the splicing technology used for the separate spans of long-span existing bridges still lacks sufficient support, and needs further study.

In this research, the existing Xinfengjiang bridge (henceforth called 'the old bridge') served as the case study. The integral splicing design method and corresponding construction technology were studied.

Firstly, the splicing requirements of the old bridge were investigated by analyzing the relative deformation difference between its two separate spans from different dimensions. Based on the results comparison of the theoretical calculation, static-load test, on-site long-term monitoring, and random traffic flow simulation, an appropriate design basis of integral splicing the old bridge was also proposed.

Secondly, an integral splicing structure for the old bridge with separate spans was proposed, and its mechanical properties were tested. A pair of semi-loop reinforcement bars were incorporated into the joint connection segment of the proposed ISC-Structure. Ultra-high-performance concrete (UHPC) was specifically developed for this application. Three full-scale model specimens were subjected to four-point flexural loading tests. Additionally, a refined simulation model was developed for size optimization of the ISC-Structure.

Finally, the key technologies of integral splicing construction were studied based on actual site conditions. A layered and segmented construction scheme tailored to the ISC-Structure was formulated. Radar equipment was applied to determine the actual layout of the prestressing wire bundles, and a local concrete chiseling scheme for the flange plate ends was formulated. In addition, a movable construction platform was designed, and reinforcement planting methods were optimized. The reasonable concrete curing duration was also determined using on-site temperature monitoring.

This research of integral splicing design and construction technology presents the following novelties. Firstly, the combined application of a direct measurement method for deformation difference between the separate spans and a simulation method utilizing traffic flow data from the freeway at the bridge site can effectively improve the rationality of splicing requirement analysis. This combined approach has not been mentioned in the current research on bridge splicing, but they are particularly important. Secondly, a novel integral splicing composite structure (ISC-Structure) was proposed. This structure realizes integral splicing between the separate spans with limited intervals, and enhances the longitudinal mechanical characteristics of the old bridge. Thirdly, construction technologies and equipment are optimized to fulfill the demands of integral splicing. In the process of implementation, the end of flange plate containing transverse prestressed wire bundles was partially chiseled.

2. Introduction of Bridge Extension Project

2.1. Old Bridge Introduction

The old bridge is located on the Heyuan to Huizhou section of G25 ChangShen Freeway. It is a three-span prestressed concrete continuous rigid-frame bridge. The bridge was constructed in 2005, and was designed in accordance with the former general specification JTJ 021-1989 [17]. Its span combination is 75 + 130 + 75 = 280 m, as shown in Figure 2a. The bridge consists of two separately constructed spans, each carrying four-lane bidirectional traffic. The cross-section layout is presented in Figure 2b. The main girder features a single-box, single-chamber cross-section. The box girder width is 1380 cm. The box girder is designed with variable cross-section height, and the cross-section height is in the range of 260 cm–700 cm. The cantilever width of the flange plate is 315 cm. The flange thickness is 108 cm at the cantilever root and 18 cm at the end. The minimum spacing between the adjacent flange ends is 40 cm.

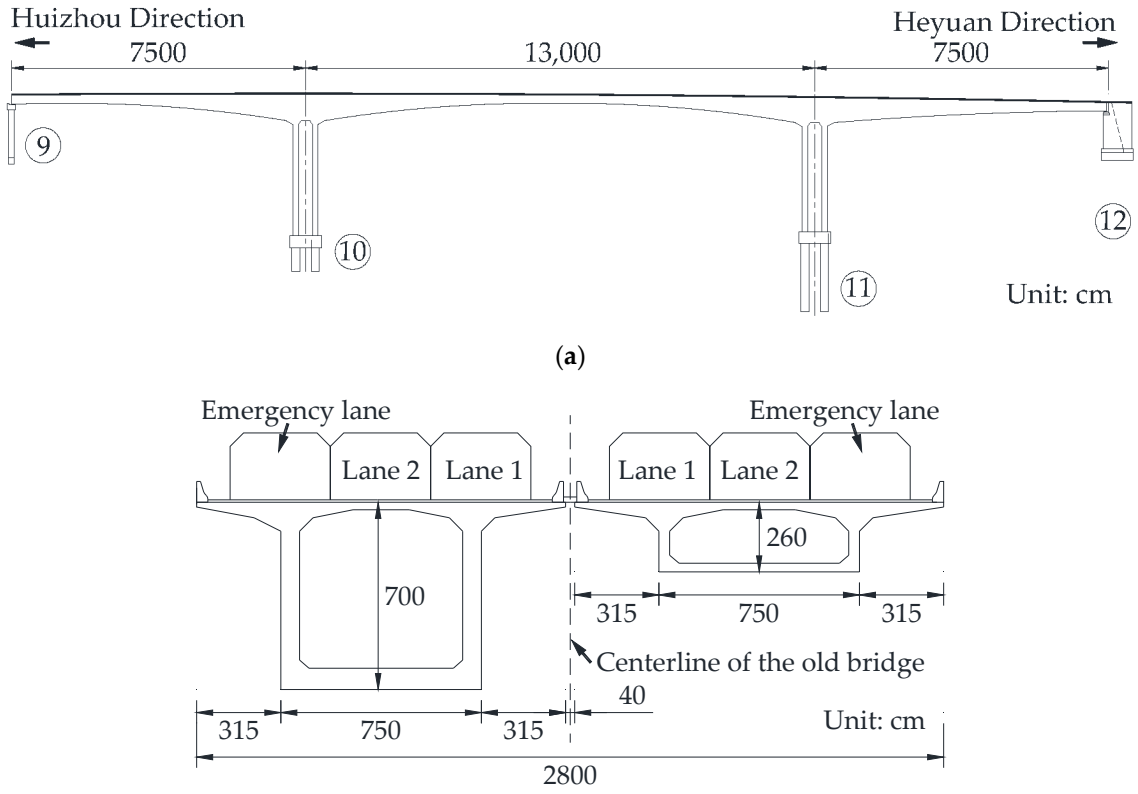


Figure 2. General layout of existing Xinfengjiang Bridge: (**a**) profile diagram; (**b**) cross-section diagram.

The main girder is prestressed with three directions. Prestressing steel wire bundles are applied in the longitudinal and transverse direction, while a prestressing ribbed bar is employed in the vertical direction. Prestressing wire bundles for the top slab and flange plate are distributed within 126 cm zones adjacent to each web side. The transverse prestressing wire bundle are spacing at 100 cm intervals along the longitudinal direction of the old bridge. Transverse prestressing is tensioned at a single end, and the tensioning and anchorage ends are staggered longitudinally. Grooves are reserved at the flange end to arrange the anchorage end of the transverse prestressing bundle. The concrete in the groove is post-poured after tensioning is completed. The prestressing arrangement at the flange end is illustrated in Figure 3.

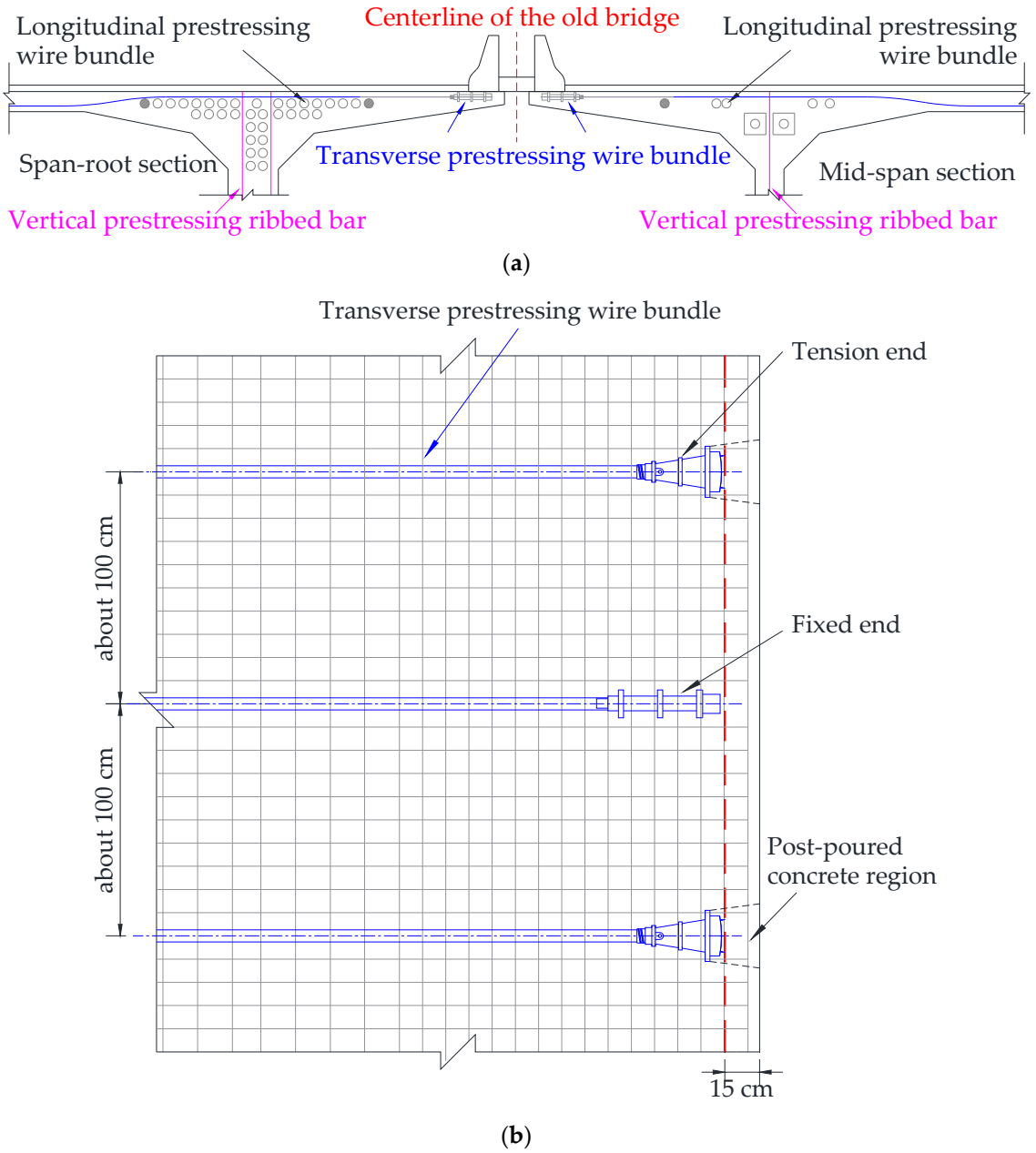


Figure 3. Arrangement of prestressing wire bundles: (**a**) cross-section diagram; (**b**) partial plan diagram of transverse prestressing wire bundle.

2.2. Bridge Extension Scheme

This G25 Heyuan Huizhou section requires extension to accommodate increased traffic flow. For the existing Xinfengjiang Bridge, the extension scheme presented in Figure 4a is adopted. In this scheme, a bridge with the same span combination is built adjacent to the old bridge, and two separate spans of the old bridge are retained. The newly built Xinfengjiang Bridge (henceforth called 'the new bridge') adopts the same structural form as the old bridge. The main girder of the new bridge adopts the single-box double-chamber cross-section, as drawn in Figure 4b. The new bridge was built in 2024, and was designed according to the new general specification JTG D60-2015 [18].

The new bridge carries the four-lane traffic for the Huizhou direction, while the old bridge will carry the four-lane traffic for the Heyuan direction. Therefore, the original bidirectional traffic on the old bridge must be merged. In order to avoid traffic congestion and potential traffic accidents occurring at the end of the old bridge (where the lane

separation exists), it is necessary to splice two separate spans of the old bridge. The two separate spans are integrated at their adjacent flange plates. This method can facilitate potential traffic crossover need. However, according to the guidelines for the design of expressway reconstruction and extension [19], the old bridge, as part of this extension project, must also meet the requirements of new general specification JTG D60-2015 [18]. The main differences between the new and former general specification are as follows: new provisions are made for the vehicle load component of the live load, and a lane load model with a simplified calculation method is proposed in the new general specification. Compared to the former general specification, the bridge structure response calculated using the lane load model of the new general specification generally results in higher values. This means that the old bridge after extension might not meet the requirements of the new general specification.

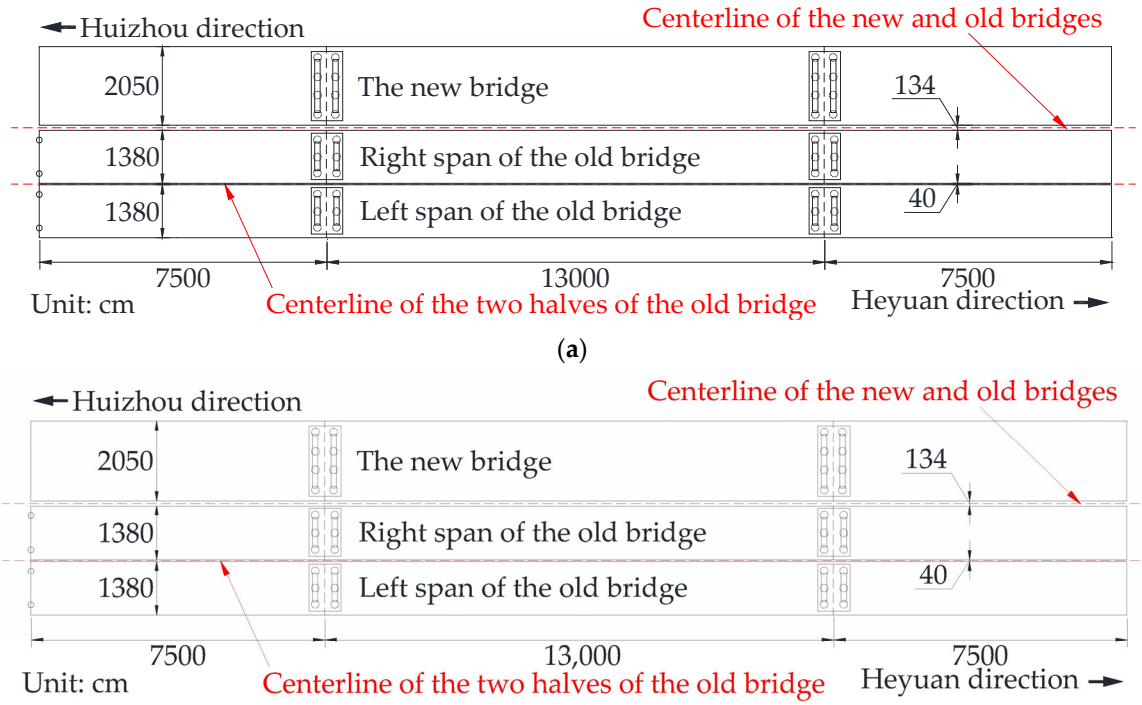


Figure 4. General layout of the extended Xinfengjiang bridge after integral splicing: (**a**) plane diagram; (**b**) cross-section diagram.

2.3. Integral Splicing Implementation Process

The implementation process for the integral splicing of a long span box girder bridge is summarized in Figure 5.

The integral splicing can be mainly divided into the following steps:

Firstly, the relative displacement difference at the splicing position should be determined. In this study, methods including theoretical calculation, load testing, field monitoring, simulation analysis, and so on are applied. A reasonable comparison of the differences between these methods is presented in Section 3.

Secondly, the dimension, material type, and mechanical properties for the integral splicing structure should also be clarified. Based on the comparison of various connection methods in this study, the integral splicing structure of the old bridge flange plate is designed according to the determined splicing displacement difference. In addition, a reasonable type of concrete material for the integrated splicing is also selected, and its material properties are tested. The mechanical properties of the integral splicing structure

are evaluated using a local model test and finite element simulation. The integral splicing scheme of box girder old bridge is reasonably verified, as detailed in Section 4.

Thirdly, the integral splicing construction of flange plates is carried out on site. Prior to construction, a layered and segmented construction scheme should be determined. A construction method suitable for on-site implementation is developed. The performance of the integral splicing implementation is monitored on site, with the results summarized in Section 5.

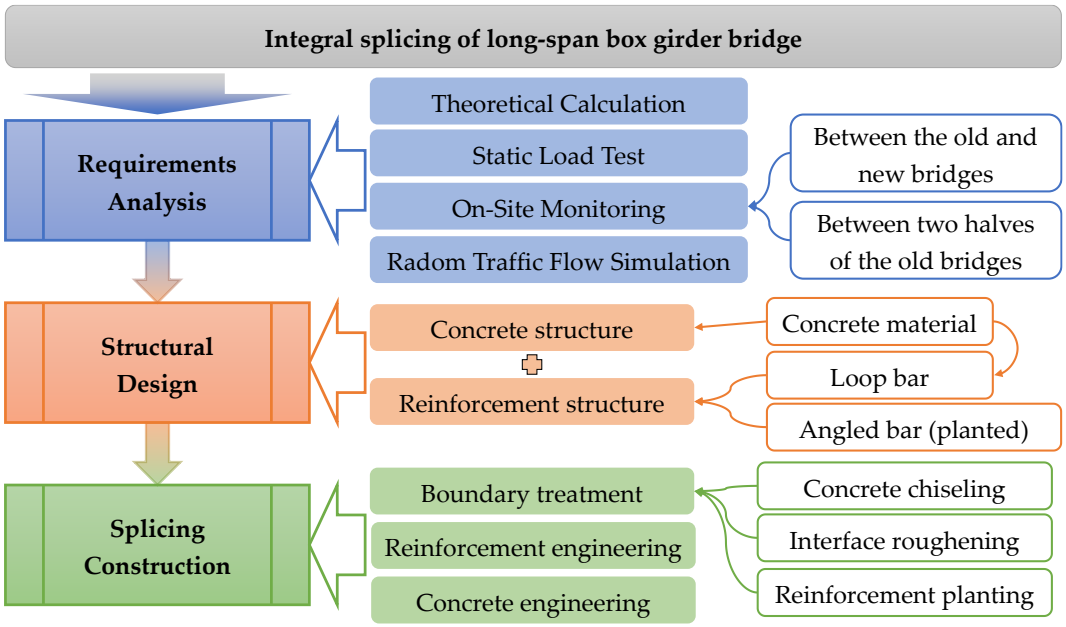


Figure 5. Main implementation process of integral splicing.

3. Splicing Requirements Analysis

In this section, various methods are adopted to clarify the actual needs of the integral splicing of the old box girder. The relative displacement differences between two separate spans of the old bridge and between the ends of the adjacent flange plates are compared and analyzed.

3.1. Theoretical Calculation and Static Load Test

The mid-span section of the second span was selected as the key section for analysis, which represents the maximum positive flexural moment condition of the middle span. A 3D simulation model of the old bridge was established, as shown in Figure 6a. The theoretical calculation results obtained according to different versions of general specifications are presented in Figure 6b.

As mentioned before, the old bridge was designed based on the old version of general specification JTJ 021-1989 [17]. According to specification JTG/T J21-01-2015 [19], the maximum test moment of the second span can be calculated based on JTJ 021-1989. Therefore, an arrangement of six standard test vehicles (36 t) is equivalently converted. The load efficiency ratio is equal to 1.03, which can meet the range of 0.95–1.05 specified in the specification JTG/T J21-01-2015.

In the process of the static load test, the method of step loading is adopted, which is divided into three levels to complete the loading of all vehicles. The bridge deformation is measured, and the deformation curve is drawn in Figure 6b. The theoretical calculation results are compared with the static load test results.

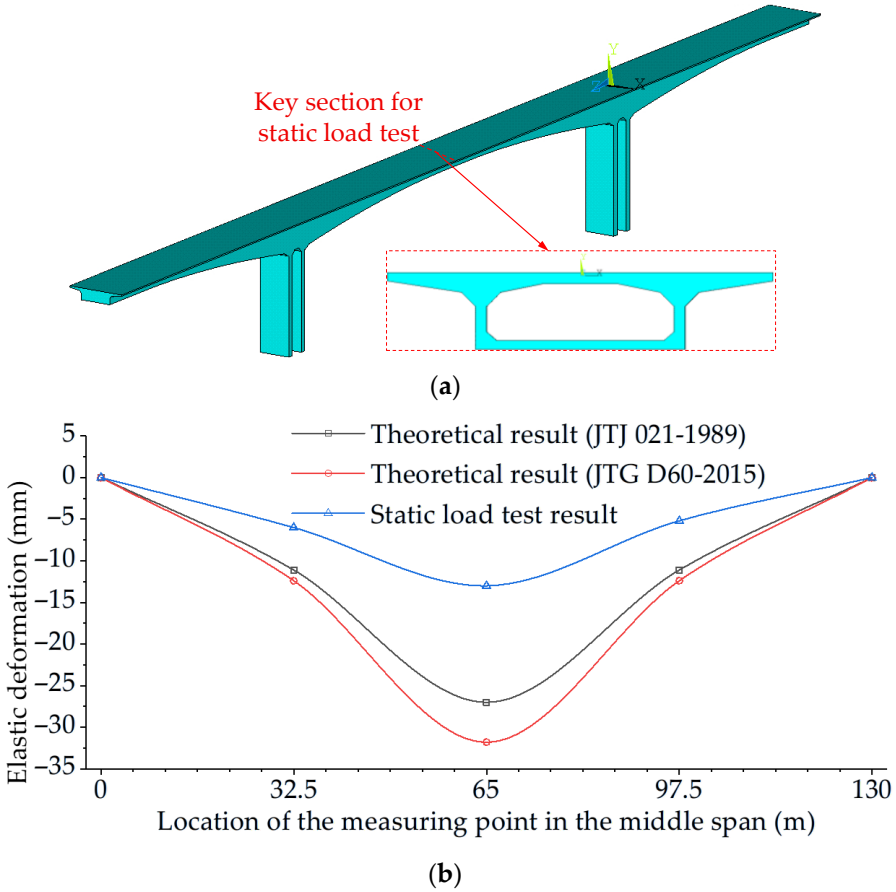


Figure 6. Theory calculation model and results comparison: (**a**) finite element simulation model; (**b**) results comparison [17,18].

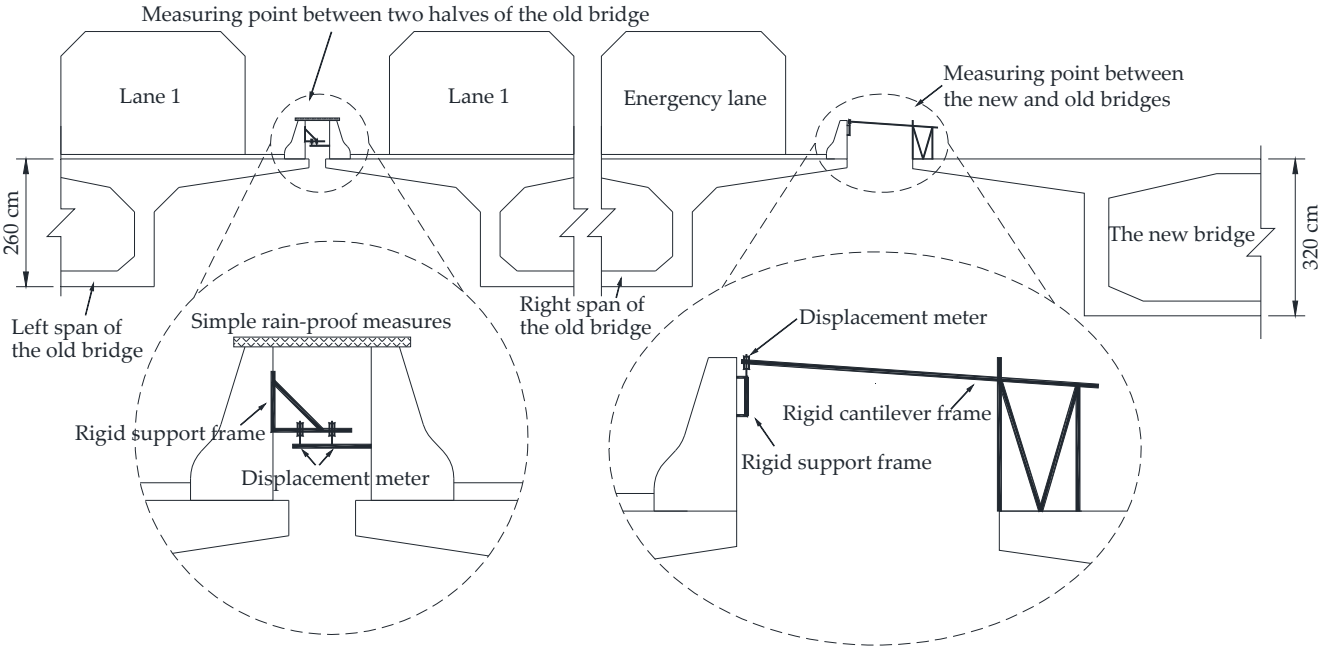
By comparing the load test results with the theoretical calculation result (JTJ 021-1989), the structural verification coefficient is in the range of 0.48–0.54, which can meet the requirements of specification JTG/T J21-01-2015. This means that the old bridge is still working in an elastic state and has sufficient performance redundancy.

In addition, the theoretical value obtained by the new general specification JTG D60-2015 [18] is compared in Figure 6b. This result is slightly larger than that of the former version. This is mainly due to the fact that the vehicle load standard is slightly improved in the new general specification.

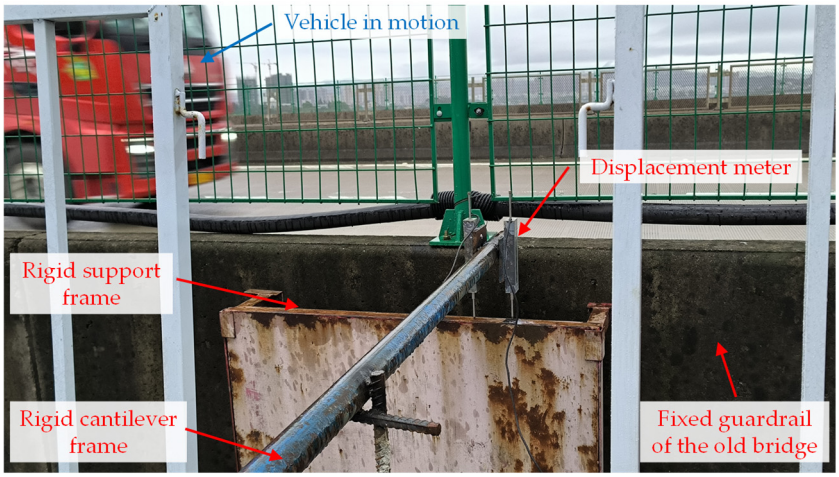
Actually, the static load test is carried out according to the most unfavorable stress principle of bridge structure. However, the vehicle load on the bridge has obvious randomness [20]. Therefore, the static test results may not reflect the actual splicing needs of the old bridge.

3.2. On-Site Monitoring and Data Analysis

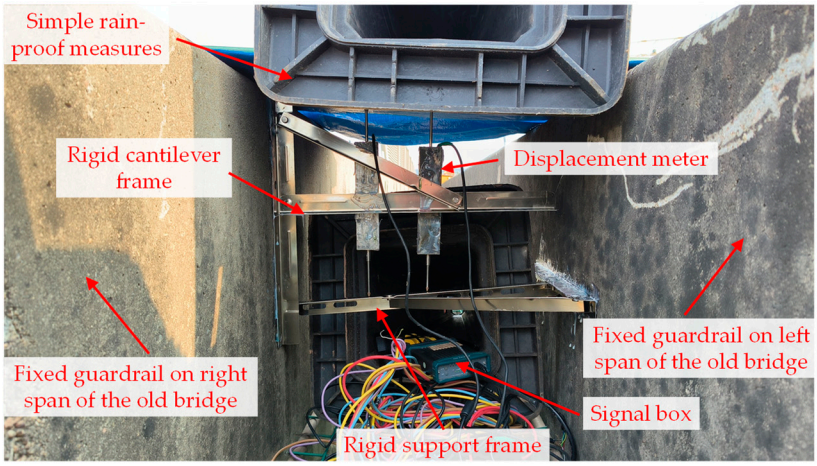
The deformation of the old bridge can be monitored by directly arranging the measuring points on site. If the measuring points are arranged at the end of the flange plate of the old bridge, the differential deformation at the splicing position can be directly measured. The mid-span section with the largest differential deformation is typically selected for the test, and the arrangement of the measuring points is shown in Figure 7a. It should be noted that the new bridge has been built, but has not yet been opened to traffic during the period of on-site monitoring. Therefore, there are no other additional loads applied to the new bridge, except for the temperature effect, in a short period of time.



(**a**)



(**b**)



(**c**)

Figure 7. Layout of on-site monitoring points: (**a**) general layout; (**b**) measuring points between new and old bridges; (**c**) measuring points between two separate spans of the old bridge.

Differential deformations between the old and new bridges and between two separate spans of the old bridge are monitored in this test. The arrangement scheme between the old and new bridges is presented in Figure 7b. At this position, a rigid cantilever frame with displacement meters is arranged at the edge of the flange plate of the new bridge. The deformation obtained can represent the deformation of a single half of the old bridge. Furthermore, the arrangement scheme between the halves of the old bridge is presented in Figure 7c. At this position, a set of rigid support frames with displacement meters is arranged between adjacent guardrails of the old bridge. The deformation obtained can represent the deformation difference between the two separate spans of the old bridge.

From 26 April 2024 to 6 May 2024, a 12-day on-site monitoring was carried out with a sampling frequency of 2 Hz. Among them, from 1 May to 3 May is the toll-free period of the freeway, and the number of vehicles passing through the old bridge was significantly larger than that in other time periods, which can be used to characterize the dense traffic flow.

The effective monitoring results of each time point are plotted as time history curves, shown in Figure 8.

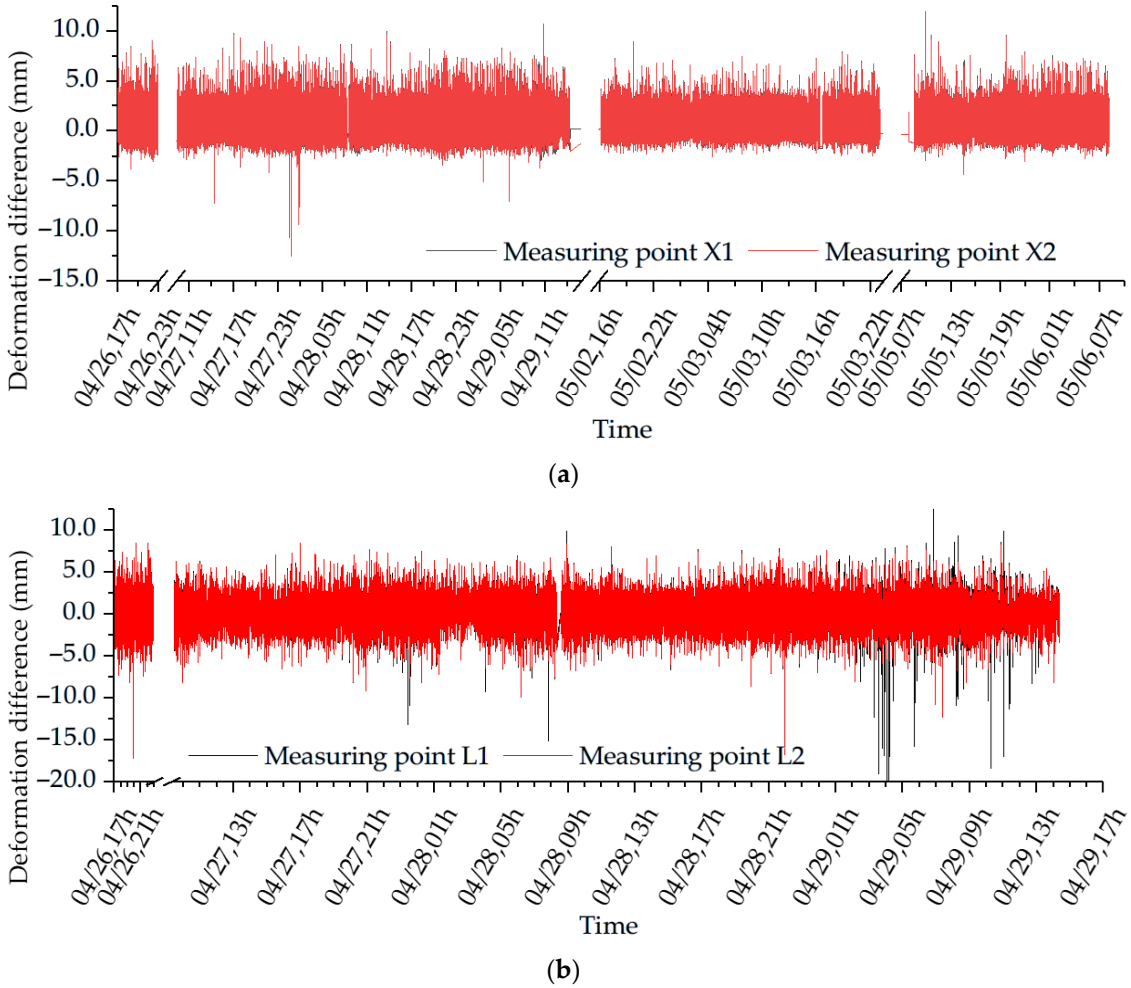


Figure 8. The displacement time history curves of on-site monitoring: (**a**) measuring points between new and old bridges; (**b**) measuring points between two separate spans of the old bridge.

In this curve, the deformation of the bridge caused by temperature effects is eliminated. It can be learnt from the statistical analysis that the frequency distribution of deformation difference generally satisfies the Pearson VII distribution. The deformation difference between the old and new bridges is mostly in the range of −2 mm–3.6 mm and concentrated in the range of −1 mm–0 mm, while the deformation difference between two separate

spans of the old bridges is in the range of ±4.2 mm and concentrated in the range of ±1 mm. Thus, the peak value of the deformation difference between the new and old bridges and that between two separate spans of the old bridges are both about 10 mm.

Although the method of obtaining the deformation difference using on-site monitoring is more direct, the length of the monitoring cycle is still limited, the monitoring cost is high, and many uncontrollable factors may have an influence. Therefore, it is necessary to introduce relevant simulation methods to further expand the test data acquisition cycle and further improve the rationality of the deformation difference value.

3.3. Random Traffic Flow Simulation

The vehicle information recorded in the freeway toll system where the bridge site is located is directly adopted. Individual vehicle characteristics information (including vehicle weight, axle number, axle load, wheelbase, etc.), overall characteristics information of the traffic flow (such as traffic volume, vehicle type composition, vehicle speed, lane selection probability, etc.), and the influence line of the key components of the target bridge can be extracted using Python 3.11.

A random traffic flow simulation method is applied, which was verified in a previous study [21]. In this method, the vehicle information obtained is converted into a simulated load sequence with spatial location, and it directly acts on the target bridge to calculate the corresponding load effect according to the specified influence line. The deformation response at the mid-span section of the old bridge is analyzed using this method. The simulation period is 400 days, and the simulation frequency is 2 Hz.

The peak deformation caused by vehicles in different lanes is extracted hourly. The probability of different deformation differences in each lane is counted in Figure 9. It can be seen from the statistical results that the random traffic flow on the emergency lane will not produce obvious displacement effects in most cases. In the case of the existing splicing deformation difference, the mean and peak values are about 4.1 mm and 9.6 mm, respectively. The mean values caused by random traffic flow on lanes 1 and 2 are about 9.7 mm and 10.9 mm, respectively. The peak values on lanes 1 and 2 are about 14.5 mm and 15.8 mm.

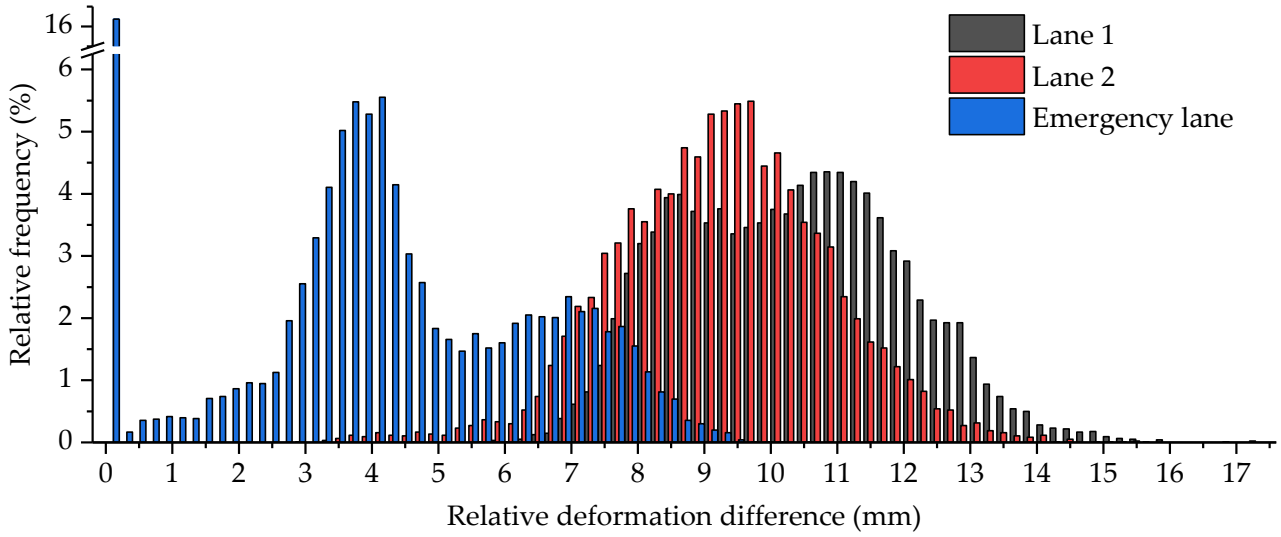


Figure 9. Statistics of random traffic flow simulation results.

3.4. Determination of Splicing Requirements

The relative deformation difference results of the old bridge obtained using the different methods mentioned above are compared in Table 1.

Table 1. Comparison of relative displacement results obtained by different methods (unit: mm).

Method		Mean Value	Peak Value
Theoretical calculation	JTJ 021-1989	27	/
	JTG D60-2015	31.8	/
Static load test		12.9	/
On-site monitoring	Between the old and new bridges	5.6	12.8
	Between two separate spans of the old bridge	8.2	18.5
Random traffic flow simulation		10.9	17.3

By comparing the results in Table 1, the following rules can be found:

Firstly, the theoretical calculation results of different specifications are significantly higher than the values obtained by other methods. This means that, in the analysis of splicing requirements, if the theoretical calculation results are directly adopted as the reference value of the integral splicing deformation, the strength of the designed splicing structure may be significantly higher than the actual demand.

Secondly, the static load test result of the old bridge is close to the peak value of the monitoring results between the new and old bridges. This indicates that the actual traffic flow on the old bridge has been close to the most unfavorable effect of the original design. However, the on-site monitoring results obtained between two separate spans of the old bridge are significantly higher than those obtained between the old and new bridges. This indicates that the tested deformation of a single old bridge cannot adequately reflect the actual deformation difference between two separate spans of the old bridge. Therefore, it is more reasonable to directly adopt the deformation difference between two separate spans of the old bridge as the design value of the integral splicing requirement.

Thirdly, the simulated value of random traffic flow is close to the on-site monitoring results between two separate spans of old bridge. The peak value of the former is only about 6% lower than that of the latter. Both can reflect the maximum deformation difference demand of integral splicing. In addition, the peak value of random traffic flow simulation is slightly higher than the mean value of the on-site monitoring results between the two separate spans of the old bridge by about 30%, which can ensure the safety redundancy of the demand for the integral splicing under normal loading conditions to a certain extent.

Therefore, for the target splicing bridge in this study, 18 mm should be considered as the design control value of the maximum deformation of the integral splicing composite structure (ISC-Structure).

4. Structural Design and Mechanical Characteristics Analysis

4.1. Structural Design

After fully investigating the relevant research results regarding the existing box girder bridge structure connection, a type of integral splicing composite structure for the long-span box girder bridge is innovatively proposed as illustrated in Figure 10.

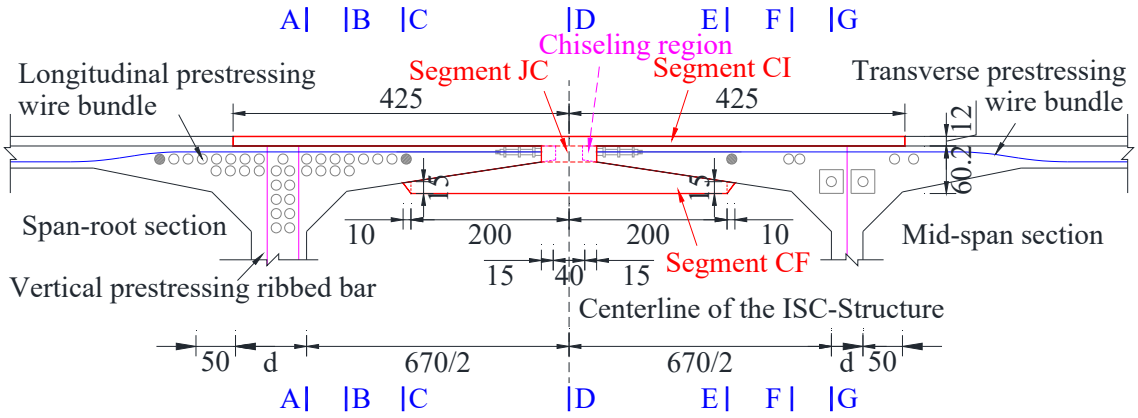
The proposed integral splicing composite structure (ISC-Structure) can be divided into three parts. From top to bottom are the composite segment serving as the integral layer (segment CI), the joint connection segment (segment JC), and the composite segment below the flange plate (segment CF), respectively. The design scheme is specified as follows:

- Composite segment as the integral layer (segment CI):

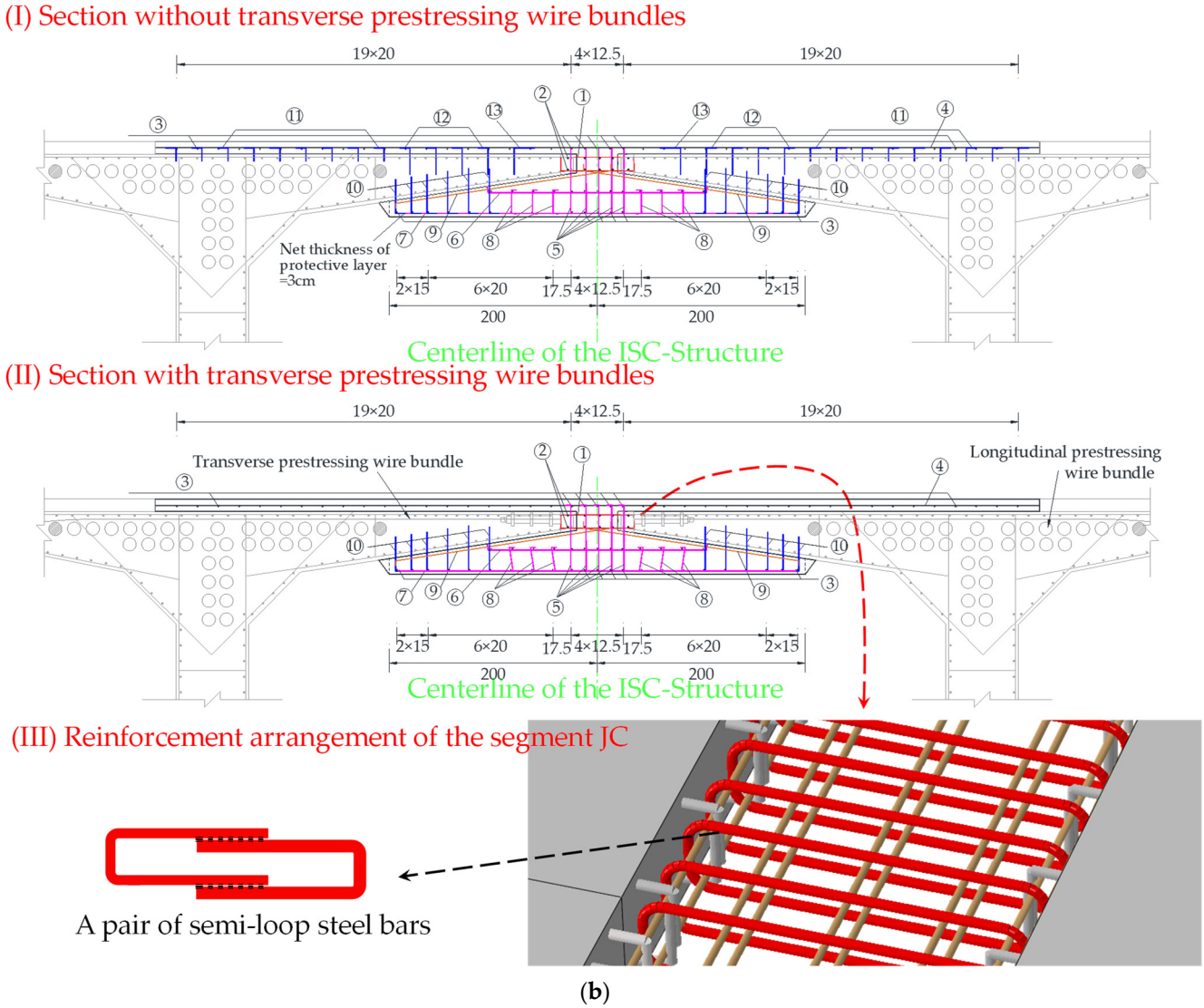
The lower surface of the segment CI should be connected to the upper edge of the flange plate of the old bridge.

The width is 2 × 425 cm, which is the distance between the inner chamfers of the adjacent webs of the old bridge.

The thickness is 12 cm, which is equal to the design thickness of the integral layer of the old bridge.



(**a**)



(**b**)

Figure 10. Structural design of proposed integral splicing composite structure: (**a**) general layout; (**b**) reinforcement layout.

- Joint connection segment (segment JC):

The width is 15 + 40 + 15 = 70 cm, of which 15 cm is the width of the concrete chiseling region at the end of the flange plate. It is determined according to the design documents and field test results.

The thickness is 20.2 cm, which is equal to the mean thickness of the flange plate at 15 cm from the end of the flange plate.

For the concrete chiseling region at the flange plate end, the concrete must be chiseled out before integral splicing, while retaining the existing steel bars in the flange plate of the old bridge.

- Composite segment below the flange plate (segment CF):

The upper surface of the segment CF is connected to the lower edge of the flange plate of the old bridge.

The standard width is 2 × 200 cm, which is determined according to the outermost position of the longitudinal steel wire bundle arranged in the flange plate.

The thickness of this segment gradually changes from the end to the center of the splicing structure. The standard thickness at the end is 15 cm, and the maximum thickness at the center is 40 cm.

In addition, a triangular decorative structure is set at the end of the segment CF to prevent the occurrence of local stress concentration at the lower edge of the flange plate.

To effectively transfer the force between the flange plate and the ISC-Structure, the following reinforcement connection measures are taken:

- Segments CI and CF:

In segment CI, the reinforcement net is formed by horizontal reinforcement and longitudinal reinforcement.

In segment CF, the reinforcement frame is composed of transverse reinforcement frame, longitudinal reinforcement and vertical reinforcement.

L-shaped anchor-bars should be planted into the flange plate surface of the old bridge to effectively connect the interface between the ISC-Structure and the flange plate surface. In particular, the position of the steel bar planted on the flange plate should not conflict with that of the existing transverse and longitudinal prestressing wire bundles.

- Segment JC:

A complete loop bar is formed in the segment JC using a pair of semi-loop reinforcement bars. It is connected to the longitudinal steel bar to form a reinforcement frame in this segment. It is also connected with the steel bar retained at the end of the flange plate after concrete chiseling so that the reinforcement of the flange plate of the old bridge and that of Segment JC can form a whole frame.

In addition, vertical reinforcement should be set among the segments CI, JC, and CF, so that the three parts of the ISC-Structure can effectively transfer forces to each other.

4.2. Material Development

In the previous study, the application of loop bars in the joint can effectively transfer the force [22]. But the lap length of loop bars needs to meet the following requirements:

$$H_{min} = s \cot\varphi \quad (1)$$

where H_{min} is the minimum lap length of loop bars; s denotes the layout spacing of the loop bar; and φ denotes the plane diffusion angle of concrete anchorage failure cone, which is closely related to the strength of the concrete.

Since the width of segment JC in the ISC-Structure proposed in this study is small, the effective lap length of loop bars is only 10 mm, which is difficult to meet the minimum requirements for lap length with normal concrete. Therefore, a new type of ultra-high-performance concrete (UHPC) is developed. The mix proportion of UHPC mixture is summarized as follows: P II 52.5 cement is 6.82 kg, S105 slag powder is 2.43 kg, silica fume is 0.49 kg, quartz sand is 14.60 kg, sulfate aluminum cement is 0.43 kg, superplasticizer is 0.23 kg, water is 2.25 kg, and steel fiber is 1.50 kg.

A material performance test of the UHPC is also carried out. The tested compressive strength is 111.3 MPa and the flexural strength is 28.0 MPa after 28 days of curing. For the old bridge after splicing, the ISC-Structure is mainly subject to the tension force, so that the ability of UHPC to resist cracking needs to be explored. A dumbbell-shaped specimen is applied to test the axial tensile performance of UHPC. The stress–strain curve of the specimen in the axial tensile performance test is shown in Figure 11.

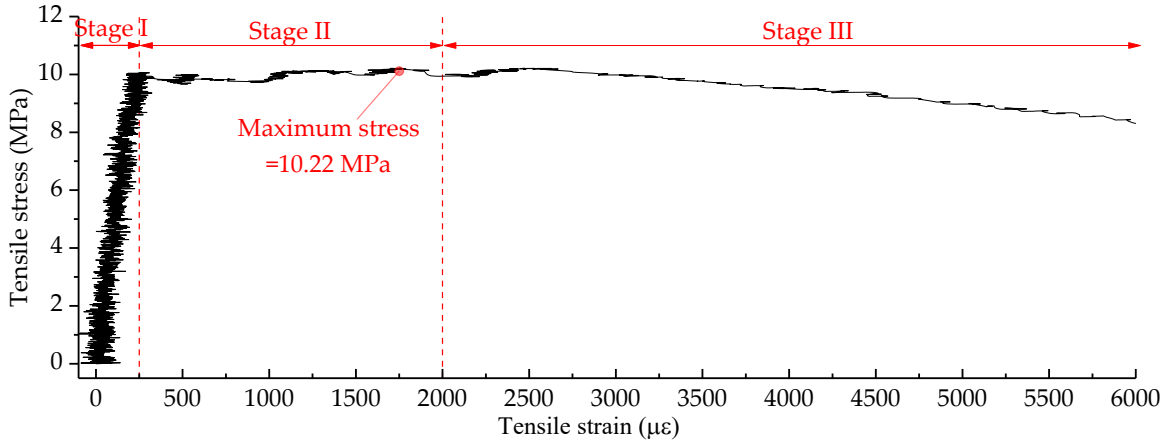


Figure 11. Tensile stress–strain relation of the adopted UHPC material.

The axial tensile strength of UHPC is 10.22 MPa, and the ultimate tensile strain is about 2000 με. The stress–strain curve can be divided into three stages:

Stage I: When the strain is less than 250 με, the relationship between stress and strain is close to linear.

Stage II: The tensile stress increases slowly, while the strain increases quickly. When the tensile strain reaches its ultimate value, the tensile stress has also reached the maximum value.

Stage III: As the strain of the material increases, the tensile stress begins to decrease slowly. The steel fiber inside the material begin to fracture quickly.

4.3. Mechanical Characteristics Analysis

4.3.1. Overall Force Characteristics Analysis

The finite element analysis model of the existing Xinfengjiang Bridge is established, as shown in Figure 12a. The mechanical properties of the old bridge before and after the implementation of the proposed ISC-Structure are calculated and compared.

Firstly, the force characteristics are analyzed from the longitudinal direction. The maximum deformation of the old bridge is compared based on different load combination regulations. According to the results listed in Table 2, the longitudinal deformation of the old bridge can be reduced by 3–6% after the implementation of the ISC-Structure. Among all kinds of loads, vehicle load has the most obvious influence, and its effect after the implementation can be directly reduced by about 42%. It can be considered, from the analysis results, that the implementation of the ISC-Structure has a certain beneficial effect on the longitudinal mechanical performance of the old bridge.

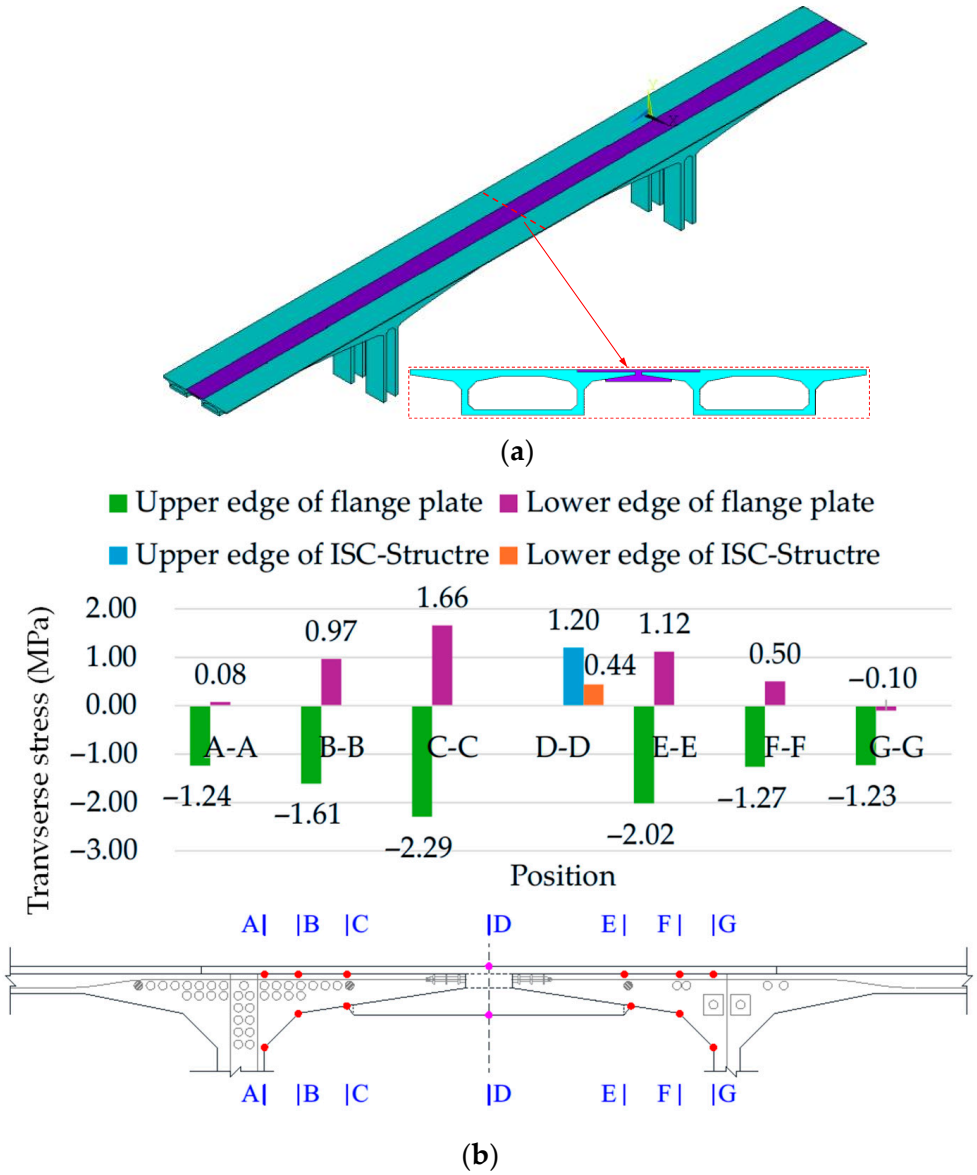


Figure 12. Mechanical characteristics analysis: (**a**) FEA model; (**b**) transverse stress distribution of flange plate after splicing.

Table 2. Analysis result of overall force characteristics (unit: mm).

Bridge State	Load Combination		Vehicle Load
	Fundamental Combination	Frequent Combination	
Before splicing	137.42	48.58	34.00
After splicing	129.50	46.88	19.85
Proportion	−5.77%	−3.50%	−41.59%

Secondly, the force characteristics are analyzed from the transverse direction. For the upper and lower edges of the flange plate after splicing, typical sections are selected, and corresponding transverse stresses are analyzed.

Taking the mid-span section with unfavorable stress as an example, the transverse stress distribution is presented in Figure 12b.

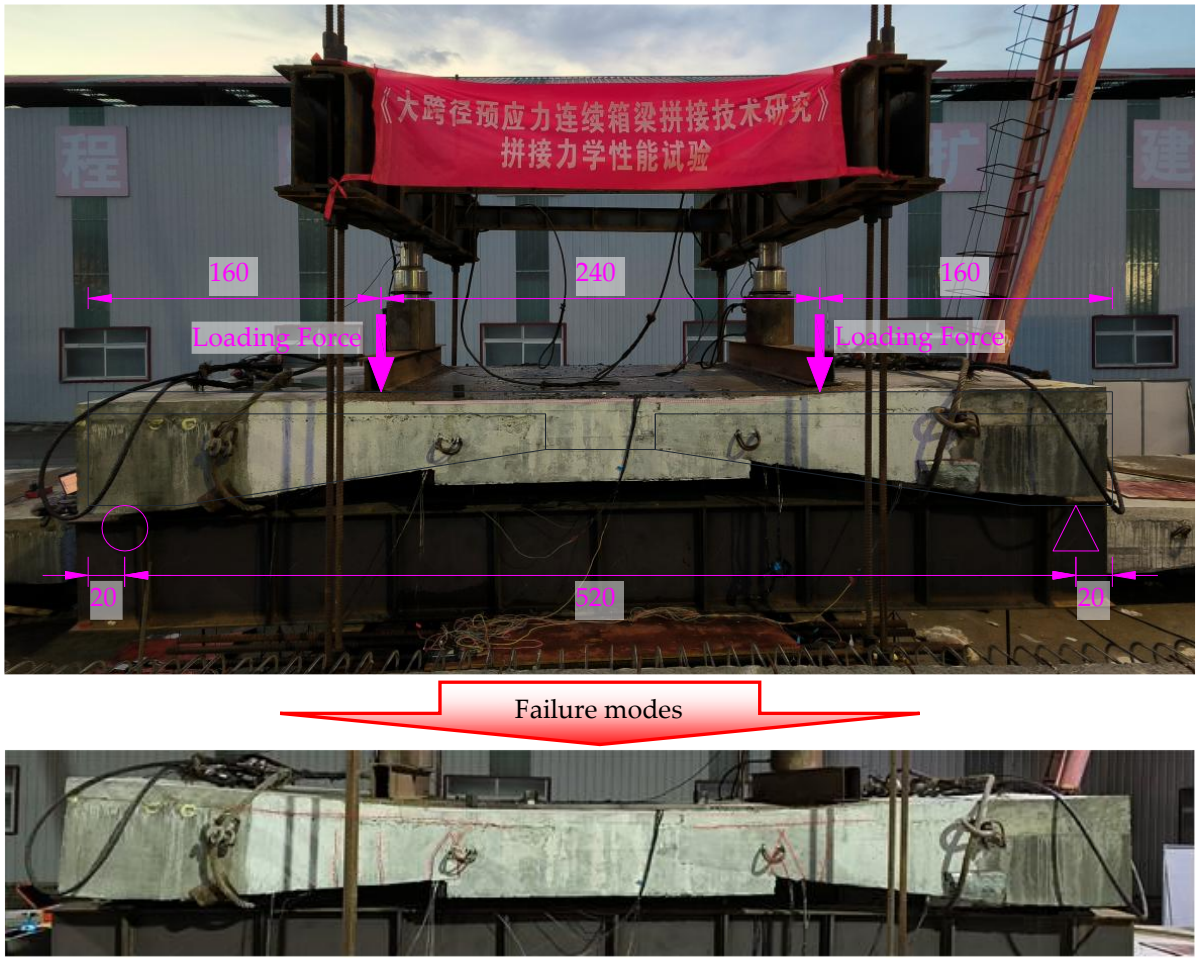
By considering the frequent combination of various loads, including the transverse prestress in the flange plate, it can be learnt that the upper edge of the flange plate is in a

state of compression. However, the maximum tensile stress at the lower edge of the flange plate is only 1.66 MPa, which can still meet the tensile strength limit of the old bridge concrete (Grade C50). It can be considered that the flange plate will not crack, theoretically, after the implementation of the ISC-Structure.

4.3.2. Local Force Characteristics Analysis

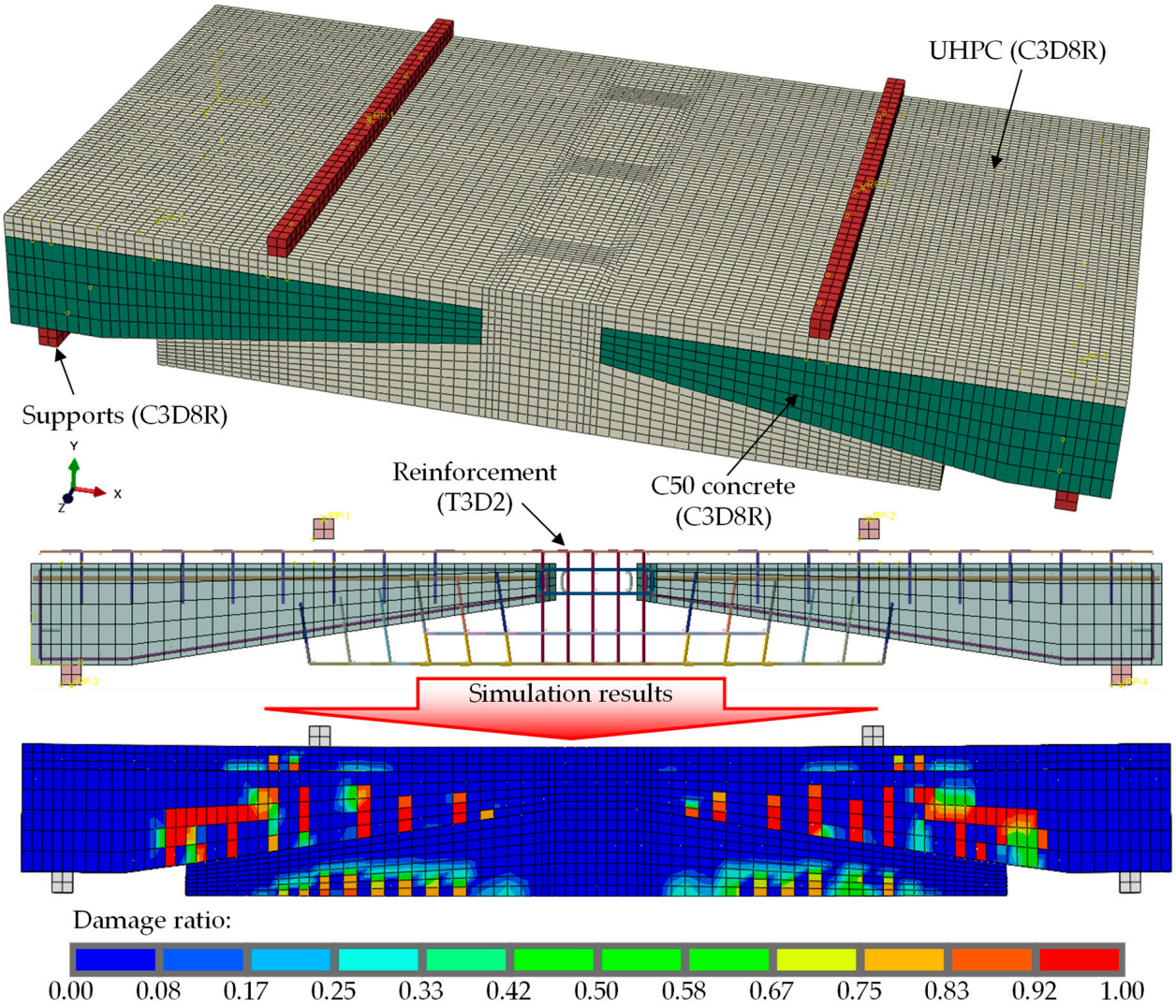
A local part of the splicing region was selected for specimen design, and three full-scale model specimens were made. The size of the specimens is 5.6 m × 3.0 m × 1.2 m. Each specimen contains two precast segments (pre-segment) and one cast-in-place segment (cast-segment). The pre-segment and the cast-segment are designed, respectively, according to the actual size of the flange plate and the proposed ISC-Structure. Each pre-segment contains three prestressing wire bundles with an adjacent spacing of 1.0 m. The specimens are fabricated according to the actual construction steps of the splicing scheme, as follows: Two pre-segments were first poured, and the prestressing wire bundles were tensioned. Then, the concrete at the end of the pre-segment was partially chiseled. Finally, steel bars in the pre-segments were planted or installed, and splicing concrete was poured.

The four-point flexural loading test was conducted on the local full-scale model specimens to test the flexural resistance of the ISC-Structure, as shown in Figure 13a.



(**a**)

Figure 13. *Cont.*



(**b**)

Figure 13. Local force characteristic analysis: (**a**) local full-scale model test; (**b**) proposed simplified simulation model and simulation result.

The test results can be summarized as follows:

1. The application of UHPC can ensure the effective lap length of the loop bar in the segment JC, but the normal concrete cannot meet the requirements.
2. Increasing the width of segment CF is beneficial to delay the interfacial debonding failure, and increasing its thickness can effectively delay the cracking of the flange plate.
3. The planted L-shaped anchor bars on the upper and lower edges of the flange plate can effectively delay the interfacial debonding failure between the flange plate and the ISC-Structure.
4. The failure mode of the ISC-Structure is as follows: the interface debonding occurs firstly, followed by cracking of the lower edge of the flange plate.

In addition, a refined simulation model for size optimization of the ISC-Structure is proposed, as presented in Figure 13b. The simulation model is built in Abaqus 6.14. The solid element of C3D8R is adopted for the concrete and supports, and the beam element of T3D2 is used for the reinforcement and the prestressed wire bundles. The element size is primarily 20 mm. The interaction between the C50 concrete and UHPC is simulated by the surface-based cohesive behavior; the reinforcements and the prestressed

wire bundles are embedded in the concrete. The prestress of prestressed wire bundles is applied using the temperature method. After running the simulation model, it can be found that the proposed simulation model can match the test results well and can meet the size optimization requirement of the ISC-Structure.

More detailed test schemes and the test and simulation results are available for reference in the published research article, 'Local Full-Scale Model Test on Mechanical Performance of the Integral Splicing Composite Structure of Adjacent Existing Box Girder Bridges' [23].

5. Integrated Splicing Construction Technology

5.1. Splicing Construction Scheme

The overall process of the integral splicing construction of the old bridge is formulated below in Figure 14.

1. Step 1: After the completion of the construction of the new bridge, the traffic of the old bridge is closed. The bidirectional traffic on the two separate spans of the old bridge is temporarily diverted to the new bridge to create favorable construction conditions for the integral splicing of the old bridge.
2. Step 2: The concrete guardrails at the splicing position are horizontally cut along the bottom of the guardrail using a diamond wire saw.
3. Step 3: Positions of the transverse prestressing wire bundles of the old bridge should be detected and marked with paint.
4. Step 4: Water-jet cutting is applied to chisel the concrete within the range of 15 cm at the end of the flange plate, but the original steel bars in the old bridge are retained.
5. Step 5: After the establishment of the construction platform, the construction of the ISC-Structure is formally carried out.

After comprehensively considering the actual condition of the splicing site and construction cost, the construction of the ISC-Structure is designed to be carried out in a layered and segmented manner. The layered and segmented construction scheme is illustrated in Figure 15.

- For the first layer, the main construction object is segments CF and JC.

The segmented construction method is adopted in this layer. The segmented length is 4.0 m. The construction direction is from the mid-span section of the second span and the beam ends to the pier regions.

Importantly, the original integral layer of the old bridge needs to be temporarily retained before the completion of the first layer. This is mainly to ensure that the stress state of the flange plate and the new segment CF will not be adversely affected by the weight change in the first layer.

- For the second layer, the main construction object is segment CI.

After the completion of the first layer, the original integral layer of the old bridge in the splicing region needs to be removed. The second layer is constructed at one time and is no longer longitudinally segmented.

The layered and segmented construction scheme is also compared with the one-time construction scheme using a simulation model. It can be observed that the adaptation of the layered and segmented construction scheme has a minor effect on the stress of the flange plate after splicing. Therefore, it is feasible to implement the integral splicing construction scheme in a layered and segmented manner.

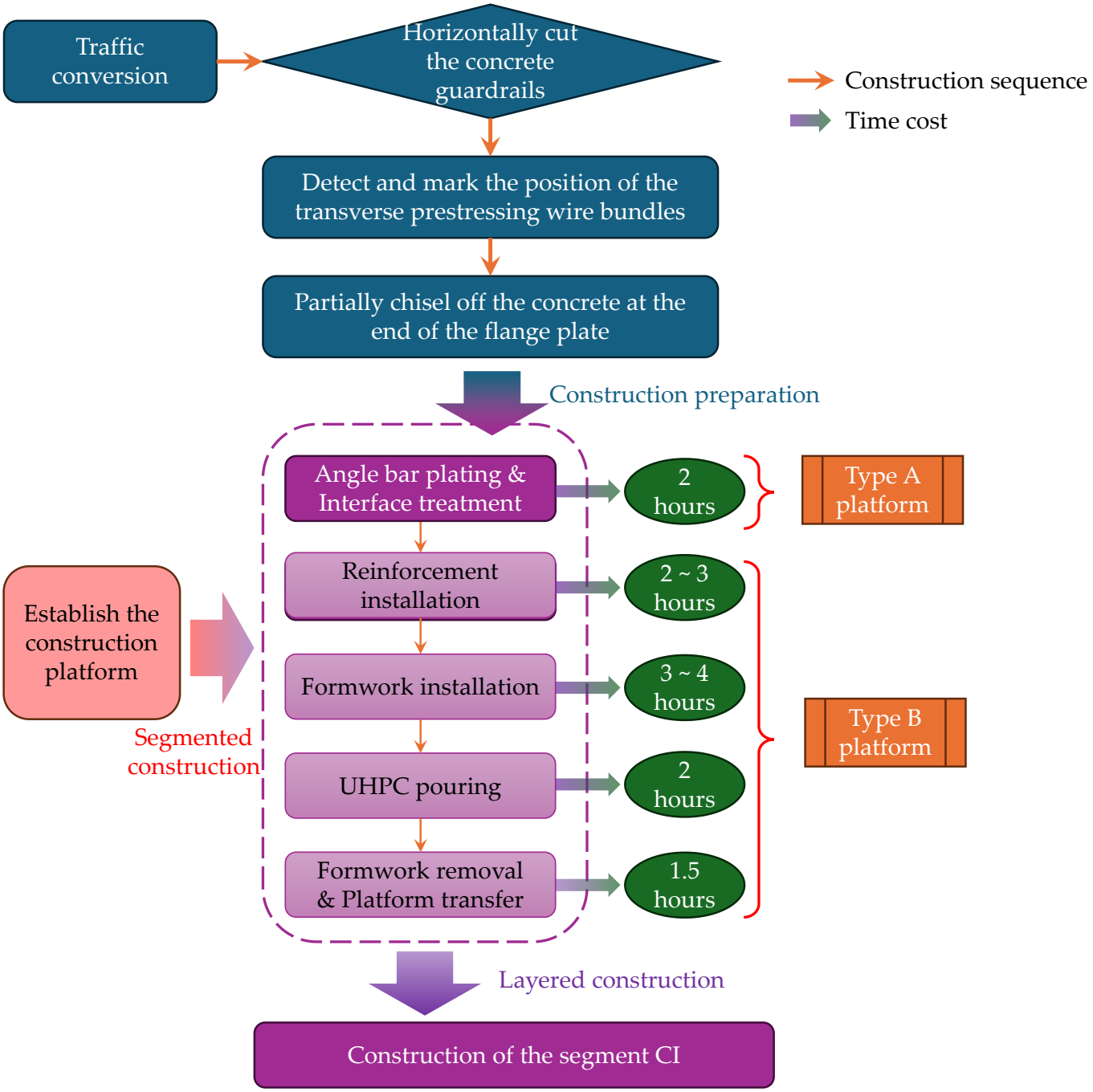


Figure 14. General process of the integral splicing construction.

When the layered and segmented construction method is adopted in the first layer, the following steps are carried out:

1. Sub-step 1: L-shaped anchor-bar planting and interface treatment. Each segment takes about 2 h.
2. Sub-step 2: Reinforcement installation. Each segment takes about 2–3 h.
3. Sub-step 3: Formwork installation. Each segment takes about 3–4 h.
4. Sub-step 4: UHPC pouring. Each segment takes about 2 h. In addition, concrete curing generally takes 18 h.
5. Sub-step 5: Formwork removal and construction platform transfer. Each segment takes about 1.5 h.

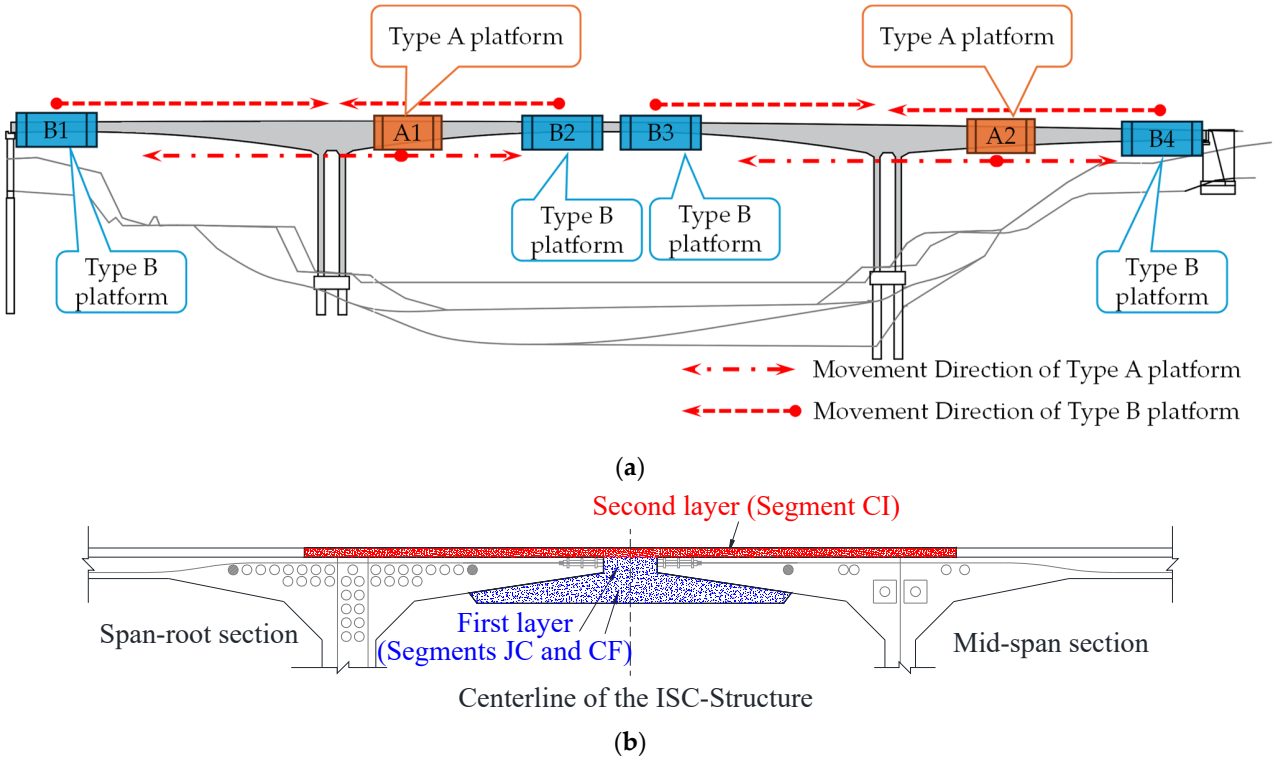


Figure 15. Integrated splicing construction scheme: (**a**) longitudinal section pouring scheme; (**b**) vertical layered pouring scheme.

5.2. Key Construction Technology

5.2.1. Position Detection of Transverse Prestressing Steel Wire Bundle

The position of the transverse prestressing wire bundles of the old bridge needs to be detected [24] for the following purposes:

Firstly, detect the anchorage position of prestressing wire bundle.

Secondly, clarify the distribution of the tension end and fixed end of the transverse prestressing wire bundles.

Thirdly, detect the reinforcement arrangement at the end of the flange plate.

Lastly, provide a reference for the L-shaped anchor-bar planting location.

Position detection was carried out using portable ground-penetrating radars, Proceq (Brand name) GP8100, at the end of the flange plate, as shown in Figure 16. This equipment adopts stepped-frequency continuous-wave (SFCW) radar, which can achieve fast target detection and excellent data acquisition of prestressing wire bundles.

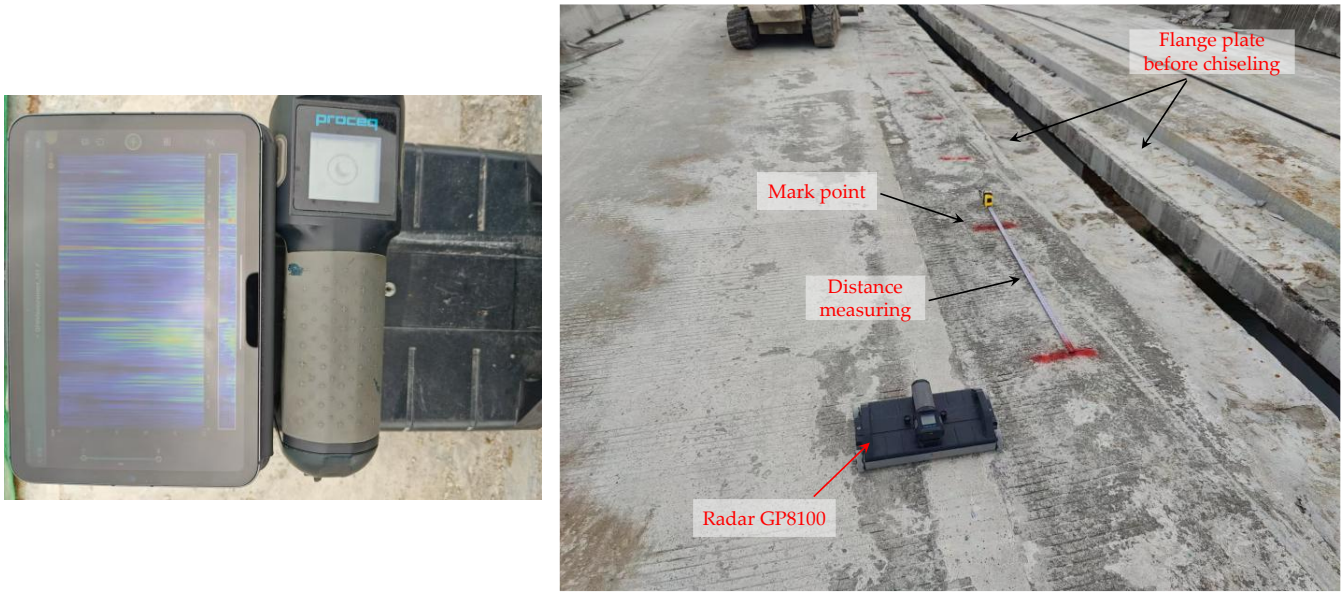
After the detection, positions were marked with red paint, as presented in Figure 16b. It was found that the actual position of the transverse prestressing wire bundle of the old bridge was basically the same as the design diagram by measuring the distance between the marking points.

5.2.2. Concrete Chiseling of Flange Plate

The concrete in the specified area at the end of the flange plate was removed using high-pressure water. The chiseling range was 15 cm (transverse) × 18 cm (vertical, minimum thickness of the end). The concrete chiseling process is shown in Figure 17a.

Before formal chiseling, the chiseling line should be marked on the flange plate. It is necessary to observe the exposure of the existing steel bar at the flange plate after chiseling. When the effective exposure length of the existing steel bar (d_s) is less than 2 cm, the chiseling range should be appropriately expanded. It should be noted that, in the process of high-pressure water chiseling, it is necessary to focus on protecting the local effectiveness

of concrete near the anchorage. Over-chiseling is strictly prohibited within the scope of the anchorage at the detected and marked position. In addition, the key section needs to be selected and the concrete strain around the prestressing wire bundle should be monitored during the chiseling operation. When there is a sudden change in the strain of concrete, the chiseling work should be stopped in time.



(**a**) (**b**)

Figure 16. Position detection of transverse prestressing steel wire bundle: (**a**) portable ground penetrating radar GP8100; (**b**) position detection and marking.



(**a**) (**b**)

Figure 17. Chiseling of the existing flange plate: (**a**) actual situation of chiseling site; (**b**) exposure of the steel bar after concrete chiseling.

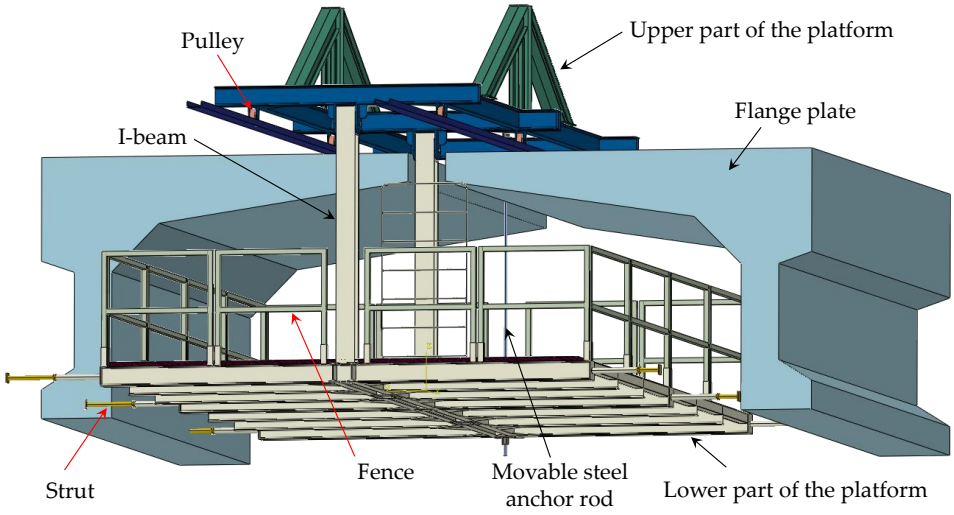
After the completion of concrete chiseling, it is necessary to observe the exposure of the steel bars at the end of the flange plate, as shown in Figure 17b. If the existing steel bar is found to be damaged or significantly deviated from the design scheme of the old bridge, it is necessary to weld new steel bars based on the existing steel bars.

5.2.3. Design of Construction Platform

Considering that the distance between the ends of adjacent flange plates is small, but the distance between the bottom of the old bridge and the water surface is large, the

construction at the lower edge of the flange plate is extremely inconvenient. Therefore, a movable construction platform is designed to facilitate the first-layer construction.

The movable construction platform is a steel truss structure, as illustrated in Figure 18. The upper part is a movable steel frame with pulleys, and the lower part is a basket structure with a fence. The upper and lower parts are connected by two I-beams and a movable steel anchor rod. When the working platform needs to be moved, the connection between the movable steel anchor rod and the platform needs to be removed. In addition, pairs of struts are added between the lower part of the working platform and the web of the old bridge to ensure the balance and stability of the platform.



(**a**)



(**b**)



(**c**)

Figure 18. Movable construction platform: (**a**) three-dimensional illustration; (**b**) upper part of the platform; (**c**) lower part of the platform.

A progressive construction sequence is adopted in the process of segmented construction. According to the time requirement of each construction sub-step, two types of movable construction platform are designed. During the splicing process of the old bridge, a total of two type-A construction platforms and four type-B construction platforms are set up, as illustrated in Figure 15a.

The type-A construction platform is mainly designed for L-shaped anchor-bar planting and interface treatment, which takes only about 2 h for each segment. The movement of the type A construction platform is bidirectional. It is arranged between the two adjacent type B construction platforms during the construction of the first layer, which is moved between the end of the side span and the mid-span of the middle span.

The type-B construction platform is mainly designed for reinforcement installation, formwork installation, UHPC pouring, and formwork removal, which takes only about 26.5 h for each segment. The movement of type B construction platform is unidirectional. They are arranged in the middle span section and side span beam end of the old bridge at the beginning of integral splicing construction. Then it moves to the pier region by-section during the construction process.

After the actual practice of the segmented construction, the average construction length of entire bridge is about 4.7 m per day.

5.2.4. Reinforcement Engineering

The reinforcement engineering of the ISC-Structure mainly includes the steel bar planting of the interface between the ISC-Structure and the flange plate, and the reinforcement engineering of the ISC-Structure.

1. Interface treatment and steel bar planting

The main construction process of interface treatment and steel bar planting is still carried out according to the construction process specified in the specification [25]. It is mainly carried out according to the following process: position marking, hole drilling, interface roughening, hole cleaning, glue injection, reinforcement installation, static curing, and quality inspection. The special points in the implementation process of the old bridge are listed below.

Firstly, for the processes of hole drilling in the first layer construction, the working surface is mainly located at the lower edge of the flange plate, and the construction workers cannot lift the heavy equipment upward for a long time [26]. Therefore, a type of special reaction support equipment is developed, as presented in Figure 19a. The bottom of the reaction support equipment can be directly supported on the ground of the construction platform, and the top of equipment can be fixed with a drilling machine. The middle of the reaction support equipment is a reaction handle, which can be pressed downward by the worker and reversely move the drilling machine upward. This reaction support equipment can directly avoid the problem of worker arm fatigue and greatly improves the efficiency of the hole drilling.

Secondly, similar problems may occur in the process of interface roughening. The optimization is carried out from two aspects, the self-weight of the roughening machine and the support equipment, as shown in Figure 19b. The traditional electric hammer is optimized into a pneumatic hammer with less weight, and a special chisel head is used for operation. Similarly, another type of special reaction support equipment is used to support the pneumatic hammer, which can also reduce the effect of worker arm fatigue during the roughening process.



Figure 19. Optimization of construction technology: (**a**) hole drilling; (**b**) interface roughening; (**c**) application of adhesion agent; (**d**) L-shaped anchor-bar positioning.

Thirdly, an interface bonding agent is adopted, as presented in Figure 19c. It should be evenly applied at the interface between the ISC-Structure and the flange plate after the completion of hole drilling and before the L-shaped anchor-bar planting. The construction quality of the interface can be ensured by considering the mechanical performance difference between the flange plate concrete and the newly poured UHPC.

Finally, the position of the L-shaped anchor-bar can be located by means of a pulling wire, as shown in Figure 19d. In addition, injection packers are applied in the process of L-shaped anchor-bar planting. It can prevent the glue from flowing out of the hole due to self-weight during its curing process, and the planting effect can also be guaranteed.

2. Reinforcement engineering of the ISC-Structure

The transverse and vertical steel bars (from No. 5 to No. 8) in the segments CF and JC are standardized welded in advance, as presented in Figure 20.

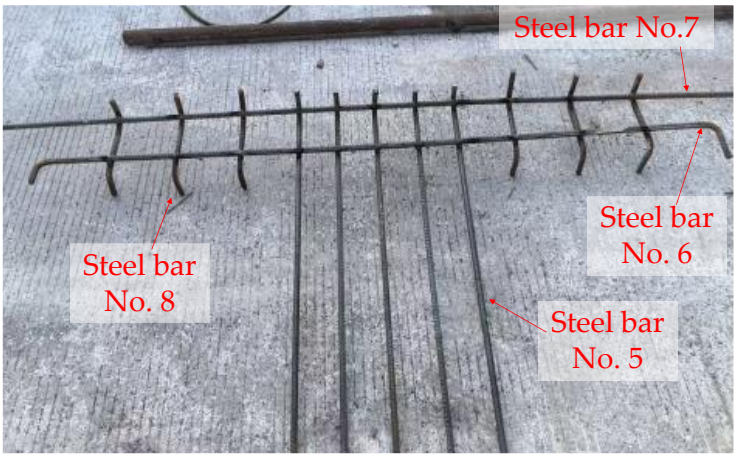
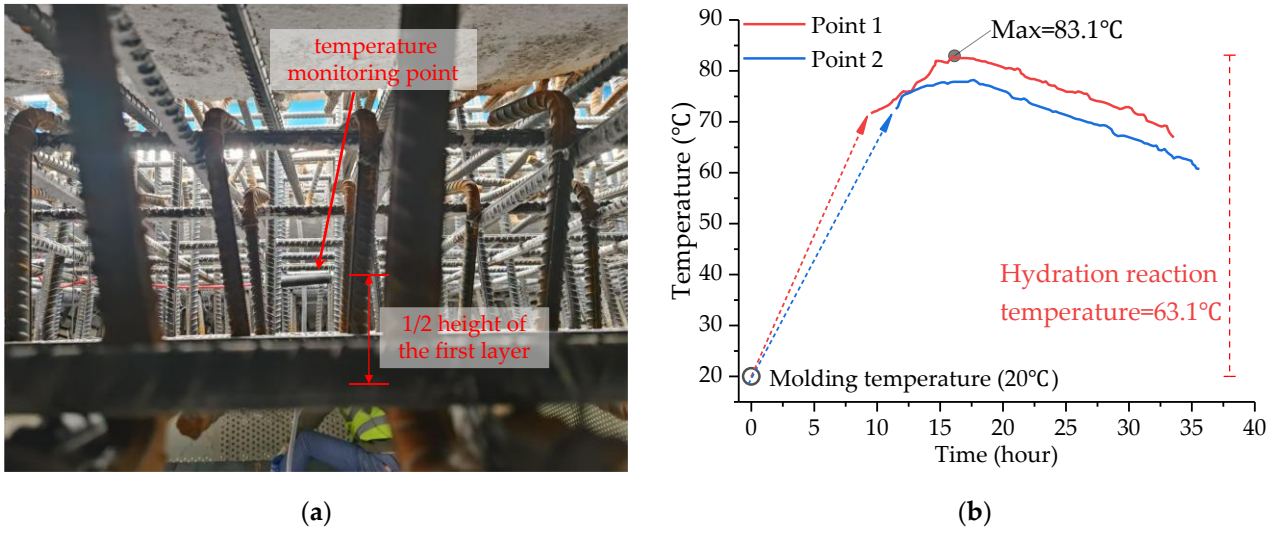


Figure 20. Modular steel skeletons applied in the splicing structure.

5.2.5. Concrete Engineering

To clarify the reasonable time and actual maintenance effect of on-site maintenance of the splicing structure, temperature monitoring the hydration heat of concrete should be carried out [27]. The layout of on-site measuring points is shown in Figure 21a, and the temperature monitoring results are illustrated in Figure 21b.



(**a**) (**b**)

Figure 21. Concrete hydration reaction monitoring: (**a**) layout scheme of measuring points; (**b**) temperature history of hydration reaction.

The results show that the molding temperature of concrete is 20 °C, and the maximum temperature of concrete during the hardening period can reach 83.1 °C. This means that the hydration heat of concrete rises by 63.1 °C. It can also be concluded that, for the concrete applied in the field, the hydration reaction lasts for a long time, and the degree of temperature rise is high.

Therefore, it is necessary to determine the reasonable timing of formwork removal in combination with weather conditions during the construction of the ISC-Structure. It is recommended to remove the formwork when the temperature difference between the interior and the environment is not greater than 50 °C. In addition, when the hydration reaction is too fast, the method of pipe cooling may be adopted for internal cooling if necessary.

5.3. Implementation Status

The implementation effects of each key construction step after adopting the above construction technology are presented in Figure 22.

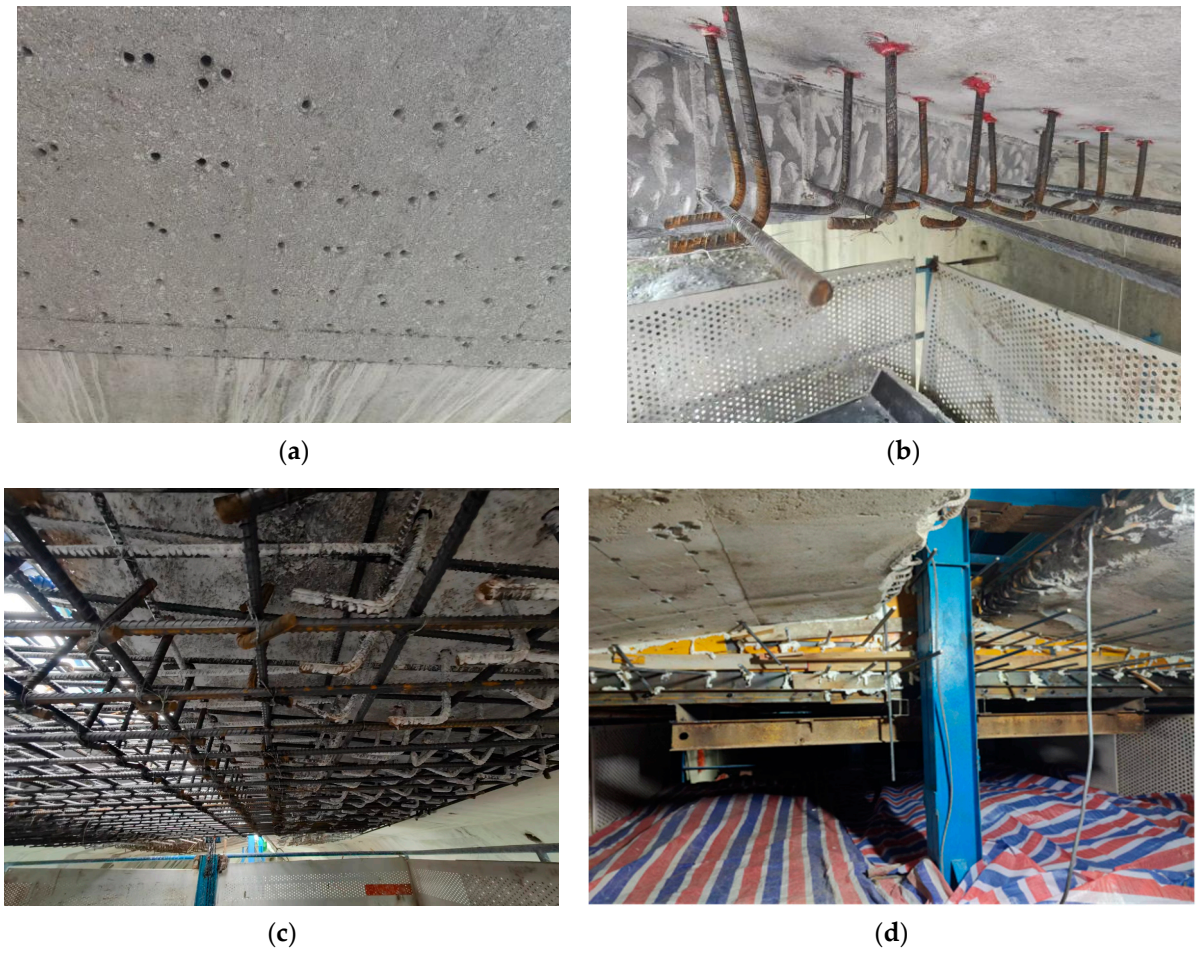


Figure 22. Implementation effect of key construction technology: (**a**) after hole drilling and interface roughening; (**b**) after bar planting; (**c**) after reinforcement binding; (**d**) after the formwork is installed.

Figure 22a shows the interface treatment effect of the lower edge of the flange plate. The treated interface is rough and can meet the construction requirement of integral splicing.

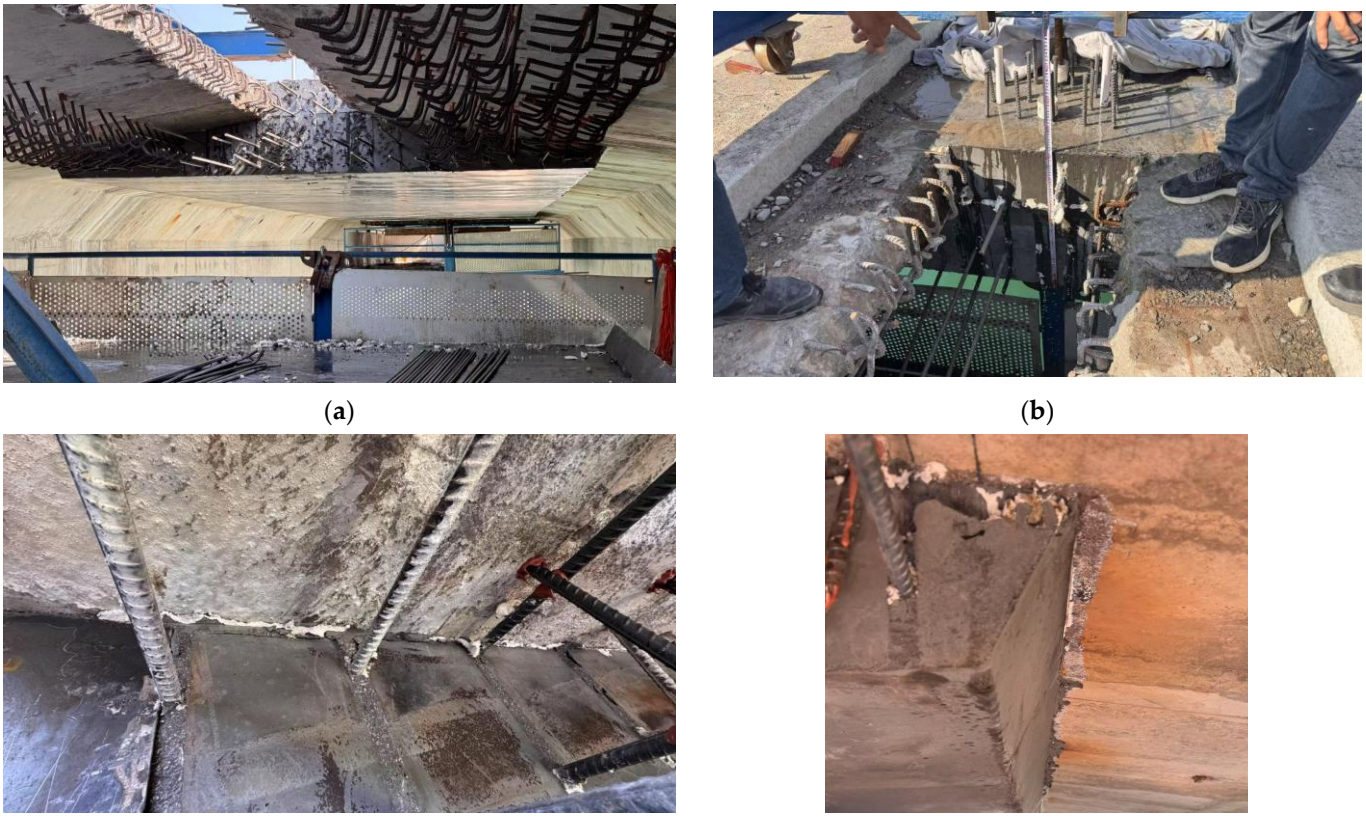
In Figure 22b, the application effect of the injection packer in L-shaped anchor-bar planting is presented. The planting position of the L-shaped anchor-bar can meet the design requirement of the ISC-Structure. The pull-out force test of the planted bars was carried out on site. The test results show that the pull-out force of the planted bars can meet the design requirements as well. This means that the effective force transmission between the ISC-Structure and the flange plate of the old bridge can be guaranteed.

In Figure 22c, the installed reinforcement of the first layer is exhibited. The arrangement position and spacing of reinforcement can meet the design requirements. With the application of modular steel skeleton, the reinforcement binding efficiency in the field can be increased from 5 h to 3 h for each segment of the ISC-Structure.

Figure 22d illustrates the steel formwork adopted in the segmented construction. The gap between the end formwork and the reserved steel bar is sealed with expanding foam sealant. And there was no obvious leakage of grout that could be observed in the UHPC pouring process.

After the maintenance of the ISC-Structure is completed, the on-site implementation effect is presented in Figure 23. The bottom surface of the ISC-Structure shown in Figure 23a:

it is flat and bright without obvious cracks. The interface between the ISC-Structure and the old bridge flange plate shown in Figure 23b is closely bonded, and no obvious interfacial cracking can be detected. In addition, it can be seen from Figure 23c and d that the surface of segmented construction segment, especially at the end of the segment CF, is dense and has no local voids.



(**a**) (**b**)

(**c**) (**d**)

Figure 23. The implementation effect after the first segment splicing: (**a**) bottom perspective; (**b**) top perspective; (**c**) cross-sectional perspective; (**d**) local perspective.

At present, the integral splicing of the existing Xinfengjiang Bridge has been completed. The apparent quality of the ISC Structure is good, and no obvious cracks and other construction quality defects can be found.

6. Conclusions

An integral splicing design and the construction technology for two separate spans of the old box girder bridge are investigated in this work. The following conclusions can be drawn:

1. The direct measurement of deformation difference between two separate spans of the old bridge is a necessary means to determine the splicing requirements. The proposed simulation method can verify and expand the amount of data measured in the field.
2. For the proposed ISC-Structure, the L-shaped anchor-bar and loop bar play important roles in connection, and the new developed UHPC is a key factor to keep the loop bar connection effective. The longitudinal force of the old bridge can be greatly improved after adopting the proposed ISC-Structure due to the composite action of the two separate spans.
3. The proposed layered and segmented construction scheme can meet the requirements of actual situations. Radar equipment can be applied to clarify the actual layout of

the prestressing wire bundles. It is feasible to carry out local concrete chiseling at the flange-plate end of the prestressed concrete box girder.

The proposed ISC-Structure has been successfully applied to practical engineering. But long-term performance monitoring of the integral spliced bridge can also be performed to evaluate its actual performance in subsequent studies.

Author Contributions: Conceptualization, C.Z. (Chunyao Zhong) and J.S.; methodology, Q.L. and Y.L.; software, J.S. and C.Z. (Chaoyu Zhu); validation, C.Z. (Chunyao Zhong), Q.L., and Y.L.; formal analysis, J.S. and C.Z. (Chaoyu Zhu); investigation, C.Z. (Chaoyu Zhu); resources, C.Z. (Chunyao Zhong); data curation, X.S.; writing—original draft preparation, Y.L. and C.Z. (Chaoyu Zhu); writing—review and editing, Q.L. and J.S.; visualization, X.S.; supervision, C.Z. (Chunyao Zhong) and Q.L.; project administration, X.S.; funding acquisition, C.Z. (Chunyao Zhong). All authors have read and agreed to the published version of the manuscript.

Funding: This research was funded by the Science and Technology Project of Guangdong Transportation Group Co., Ltd. (Grant No. JT2021YB12), and the Science and Technology Plan Project of Guangdong Province (Grant No. 2021B1111610002).

Institutional Review Board Statement: Not applicable.

Informed Consent Statement: Not applicable.

Data Availability Statement: All data are available within the manuscript.

Acknowledgments: Thanks are extended to the anonymous reviewers whose suggestions improved this manuscript.

Conflicts of Interest: Authors Chunyao Zhong, Qiao Lu and Yangfan Li are employed by the Guangdong Provincial Freeway Co., Ltd. The remaining authors declare that the research was conducted in the absence of any commercial or financial relationships that could be construed as a potential conflict of interest.

References

1. Jiang, X.; Fu, Y.; Li, L.; Gu, H.; Qiu, Y. Design Optimisation Analysis of Isolating Wall for Separated Widening Embankment on Soft Ground. *Balt. J. Road Bridge Eng.* **2021**, *16*, 2. [CrossRef]
2. ACI. *Guide for Widening Highway Bridges, Manual of Concrete Practice*; American Concrete Institute: Farmington Hills, MI, USA, 1998.
3. Zhou, J.; Lu, Z.; Zhou, Z. Structural Safety Assessment and Traffic Control Strategies of Widened Highway Bridges under Maintenance Works Requiring Partial Lane Closure. *KSCE J. Civil Eng.* **2022**, *26*, 4. [CrossRef]
4. Liu, Y.; Qian, Z.; Xie, Y.; Xu, S. Investigation on materials for prefabricated bridge deck pavement and construction technology: Application to a case study of concrete box-girder bridge. *Case Stud. Constr. Mater.* **2024**, *20*, e03185. [CrossRef]
5. Mochtar, K.; Saputra, S.Y. Expansion joint technology in bridge: A review. *Int. J. Multidiscip. Res. Growth Eval.* **2023**, *4*, 584–589. [CrossRef]
6. Liu, Z.; Phares, B.M.; Greimann, L.F. Use of Longitudinal Expansion Joints in Wide-Bridge Applications to Reduce Deck Cracking. *J. Bridge Eng.* **2013**, *21*, 10. [CrossRef]
7. Li, S.; Lv, Z.; Wang, X.; Xing, Y.; Zou, J.; Huang, C. Analysis method and theoretical research of longitudinal and transverse cross expansion joint structure. *Highway* **2024**, *69*, 3. (In Chinese)
8. Wang, J.; Huo, T.; Wang, D.; Zhang, P. Study on Basic Pavement Performance of High-Elasticity Asphalt Concrete. *Polymers* **2024**, *16*, 2156. [CrossRef]
9. Swanson, B.J.; Malla, R.B.; Shaw, M.T. Laboratory Testing, Field Installation, and Monitoring of a Silicone Foam Sealant for Bridge Expansion Joints. *J. Bridge Eng.* **2012**, *18*, 8. [CrossRef]
10. Lu, P.; Wang, J.; Ding, J.; Wu, Y.; Yang, L.; Gu, Z. Mechanical behaviour of bridge expansion joint interfaces filled with novel polyurethane-modified asphalt. *Road Mater. Pavement Des.* **2025**, *26*, 5. [CrossRef]
11. Tan, Z.; Yu, J.; Zhang, S. A Multi-Technique Hybrid Method for the Widening and Splicing of New and Old Beam Bridges. *Sustainability* **2024**, *16*, 6164. [CrossRef]
12. Chen, D.; Song, J.; Zhu, C. Development and application of anti-differential disturbance concrete for widening bridge. In *Bridge Maintenance, Safety, Management, Digitalization and Sustainability*, 1st ed.; Jensen, B.S., Frangopol, D.M., Schmidt, J.W., Eds.; CRC Press: Boca Raton, FL, USA, 2024; pp. 216–225. [CrossRef]

13. Wu, W.; Cao, C.; Wu, Y.; Liu, J.; Liu, D.; Chen, L.; Liu, Z. Numerical Analysis on Sliding-Type Transverse Splicing Connection Applied in Widening Continuous Concrete Box-Girder Bridge. *Buildings* **2025**, *15*, 35. [CrossRef]
14. Wu, W.; Zhang, H.; Liu, Z.; Wang, Y. Numerical Analysis on Transverse Splicing Structure for the Widening of a Long Multi-Span Highway Concrete Continuous Box Girder Bridge. *Materials* **2022**, *15*, 6805. [CrossRef]
15. Liu, S.; Yu, L.; Han, H.; Pan, F.; Wu, K.; Yang, Z. Effect of Vehicle–Bridge Coupled Vibration on the Performance of Magnesium Phosphate Cement Repair Materials. *Materials* **2021**, *14*, 7743. [CrossRef]
16. Gu, P.; Wu, H.; Li, L.; Li, Z.; Hong, J.; Zhuang, M.-L. Effect of Traffic Vibration on Compressive Strength of High-Strength Concrete and Tensile Strength of New-to-Old Concrete Interfaces. *Building* **2024**, *14*, 3765. [CrossRef]
17. *JTJ 021-1989*; General Specification for Design of Highway Bridges and Culverts. China Communication Press: Beijing, China, 1989. (In Chinese)
18. *JTG D60-2015*; General Specification for Design of Highway Bridges and Culverts. China Communication Press: Beijing, China, 2015. (In Chinese)
19. *JTG/T J21-01-2015*; Load Test Methods for Highway Bridges. China Communication Press: Beijing, China, 2011. (In Chinese)
20. Zhao, L.; Yang, Z.; Tong, X.; Zhang, Y.; Nie, R. Experimental Study on Fatigue Characteristics and Life Prediction of Rotating Restricted Short Suspender in Suspension Bridge. *Buildings* **2025**, *15*, 254. [CrossRef]
21. Chen, D.; Zhu, C.; Shi, X.; Song, J. Influence of Random Vehicle–Bridge Coupling Vibration on the Anti-Disturbance Performance of Concrete Materials. *Appl. Sci.* **2023**, *13*, 7584. [CrossRef]
22. Joergensen, H.B.; Hoang, L.C. Tests and limit analysis of loop connections between precast concrete elements loaded in tension. *Eng. Struct.* **2013**, *52*, 558–569. [CrossRef]
23. Zeng, G.Q.; Wang, X.; Shi, X.; Zhu, C.; Song, J. Local Full-Scale Model Test on Mechanical Performance of the Integral Splicing Composite Structure of Adjacent Existing Box Girder Bridges. *Buildings* **2025**, *15*, 411. [CrossRef]
24. Liu, H.; Lin, C.; Cui, J.; Fan, L.; Xie, X.; Spencer, B.F. Detection and localization of rebar in concrete by deep learning using ground penetrating radar. *Autom. Constr.* **2020**, *18*, 103279. [CrossRef]
25. *JTG/T J23-2008*; Technical Specifications for Strengthening Construction of Highway Bridges. China Communication Press: Beijing, China, 2008. (In Chinese)
26. Tian, J.; Jiang, X.; Yang, X.; Li, L.; Li, J. Study on shear mechanisms of UHPC-NC reinforced interfaces and grooved & reinforced interfaces. *Case Stud. Constr. Mater.* **2025**, *23*, e04982. [CrossRef]
27. Li, X.; Yu, Z.; Chen, K.; Deng, C.; Yu, F. Investigation of temperature development and cracking control strategies of mass concrete: A field monitoring case study. *Case Stud. Constr. Mater.* **2023**, *18*, e02144. [CrossRef]

Disclaimer/Publisher's Note: The statements, opinions and data contained in all publications are solely those of the individual author(s) and contributor(s) and not of MDPI and/or the editor(s). MDPI and/or the editor(s) disclaim responsibility for any injury to people or property resulting from any ideas, methods, instructions or products referred to in the content.